Active deformation of the Corinth rift, Greece: Results from repeated Global Positioning System surveys between 1990 and 1995

Pierre Briole, Alexis Rigo, H. Lyon-Caen, Jean Claude Ruegg, K. Papazissi, C. Mitsakaki, A. Balodimou, G. Veis, D. Hatzfeld, Anne Deschamps

JOURNAL OF GEOPHYSICAL RESEARCH, VOL. 105, NO. B11, PAGES 25,605–25,625, NOVEMBER 10, 2000

Active deformation of the Corinth rift, Greece: Results from repeated Global Positioning System surveys between 1990 and 1995

P. Briole,[1] A. Rigo,[2] H. Lyon-Caen,[3] J. C. Ruegg,[1] K. Papazissi,[4]
C. Mitsakaki,[4] A. Balodimou,[4] G. Veis,[4] D. Hatzfeld,[5] and A. Deschamps[6]

Abstract. Between 1990 and 1995, we carried out seven Global Positioning System (GPS) campaigns in the Corinth rift area in order to constrain the spatial and temporal crustal deformation of this active zone. The network, 193 points over ~10,000 km^2, samples most of the active faults. In order to estimate the deformation over a longer period, 159 of those points are also Greek triangulation pillars previously measured between 1966 and 1972. Two earthquakes of magnitude 6.2 and 5.9 have occurred in the network since it was installed. The extension rate deduced from the analysis of the different GPS data sets is 14 ± 2 mm/yr oriented N9°E in the west, 13 ± 3 mm/yr oriented S-N in the center, and 10 ± 4 mm/yr oriented N19°W in the east of the gulf. The comparison between GPS and triangulation gives higher rates and less angular divergence (25 ± 7 mm/yr, N4°E; 22 ± 7 mm/yr, S-N; 20 ± 7 mm/yr, N15°W, respectively). Both sets of data indicate that the deforming zone is very narrow (10-15 km) in the west, might be wider in the center (15-20 km), and is more diffuse in the east. The analysis of the displacements observed after the M_s=6.2, June 15, 1995, and the M_s=5.9, November 18, 1992, earthquakes, both located in the west of the gulf, together with seismological and tectonic observations shows that these two earthquakes occurred on low-angle (≤ 35°) north dipping normal faults located between 4.5 and 10 km depth in the inner part of the rift. Assuming that the deformation is concentrated in relatively narrow deforming zones, we use a simple model of a dislocation in an elastic half-space to study the implication of the localization. Using the geometry of the known seismogenic faults, our observations imply continuous aseismic deformation in the uppermost crust of the inner rift. This model predicts geodetic strain rates close to seismic strain rates in opposition to previous estimates. This is because our model takes into account the activity on low-angle normal faults in the inner rift and an effective seismogenic layer of 6-7 km, about half that usually assumed.

1. Introduction

The Aegean is the most seismically active part of Europe and one of the most rapidly extending provinces of the world. [e.g., *Mercier et al.*, 1977; *McKenzie*, 1978; *Le Pichon and Angelier*, 1981; *Jackson and McKenzie*, 1988; *Le Pichon et al.*, 1995]. In northern Greece the deformation is accommodated across a series of extending grabens (North Aegean trough, Evvia graben, Corinth rift) delimited by active normal faults oriented NW-SE to E-W. These grabens connect the western part of the North Anatolian fault to the Hellenic Arc [*Armijo et al.*, 1996]. The Corinth rift (Figure 1) is the most active of these grabens and the most accessible one to observations because only its central part is presently under sea level. It thus provides a very good opportunity to study in detail crustal deformation processes involved in such active rifting. The work presented in this paper is part of a European multidisciplinary effort aimed at a better understanding of these processes in that area. Results from seven Global Positioning System (GPS) campaign measurements of a dense network first installed in 1990 and now covering the entire gulf are given. Besides providing accurate in-

[1]Département de Sismologie, UMR-CNRS 7580, Institut de Physique du Globe, Paris, France.
[2]Groupe de Recherche en Géodésie Spatiale, Observatoire Midi Pyrénées, Toulouse, France.
[3]Laboratoire de Géologie, Ecole Normale Supérieure, Paris, France.
[4]Higher Geodesy Laboratory, National Technical University, Athens, Greece.
[5]Laboratoire de Géophysique Interne et Tectonophysique, Observatoire de Grenoble, Grenoble, France.
[6]Laboratoire de Géodynamique, CNRS Sophia-Antipolis, Valbonne, France.

Paper number 2000JB900148.
0148-0227/00/2000JB900148$09.00

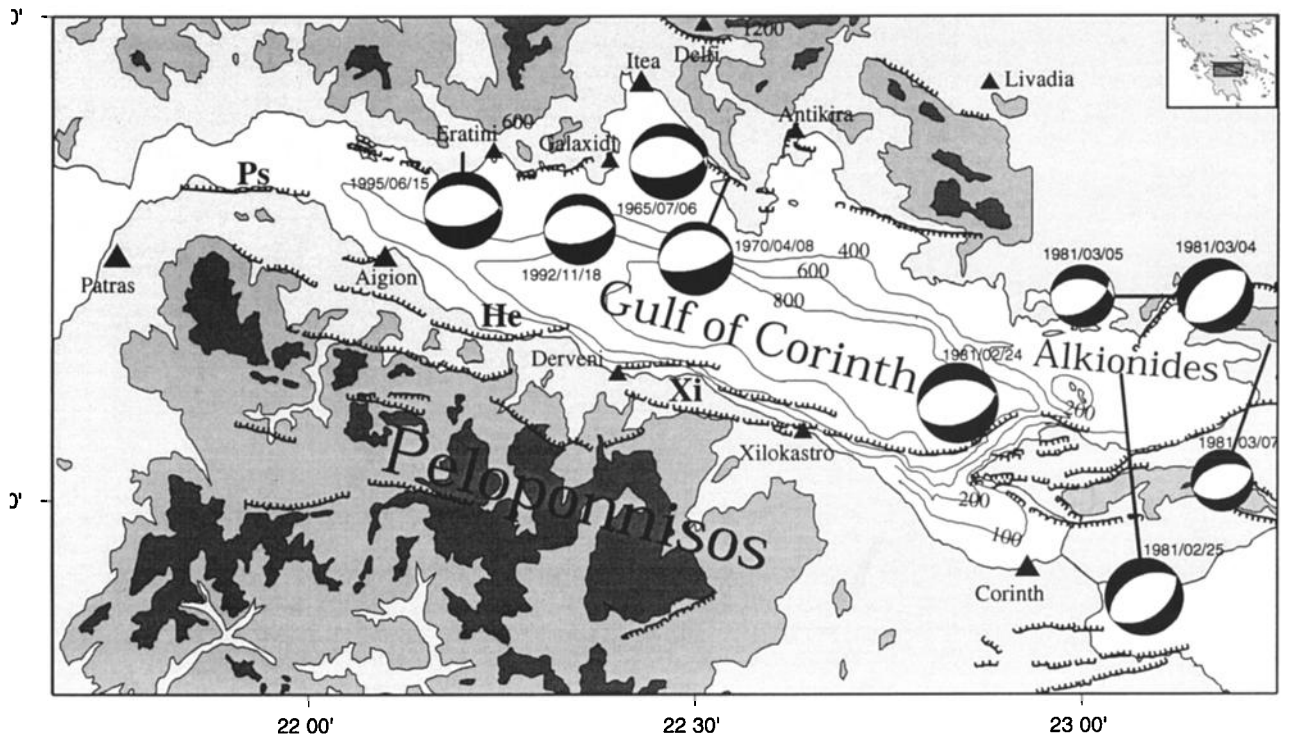

Figure 1. Seismotectonic map of the Corinth rift showing topography, active faults, and fault plane solutions of earthquakes $\geq M_s = 5.5$ for the period 1965 to present. Adapted from *Armijo et al.* [1996], *Rigo et al.* [1996], *Bernard et al.* [1997a], and *Baker at al.* [1997]. Fault plane solution parameters are listed in Table 3. Ps, He, and Xi refer to the Psatopirgos, Helike, and Xilokastro faults, respectively.

stantaneous extension rates across the rift, the density of observations both in space and time allows us to give new insights on the localization of the deformation, the effective thickness of the brittle crustal layer, and the relation between the continuous part of the deformation (loading process) and the discontinuous part associated with earthquakes. For this purpose, we use available geodetic, tectonic, and seismological observations outlined below.

The Corinth rift is an asymmetric Quaternary rift. The most active normal faults are located on the southern coast of the gulf which is subject to uplift [*Sébrier,* 1977; *Armijo et al.,* 1996]. The typical length of the E-W striking en échelon fault segments along the southern coast of the gulf (from Xilokastro to Psathopirgos) is 15 ± 5 km. Tectonic studies based on deformation modeling of marine terraces in the footwall of the Xilokastro fault, a major fault on the central part of the south coast (Figure 1), indicate that the overall long-term morphology of the southern coast of the gulf can be explained by the repetition of earthquakes on 40°-60° north dipping faults, slipping at 11 ± 3 mm/yr [*Armijo et al.,* 1996]. This would correspond to an extension rate of 6 ± 1 mm/yr. The level of historical and instrumental seismicity is quite high [*Papazachos and Papazachos,* 1989; *Ambraseys and Jackson,* 1990; *Rigo et al.,* 1996; *Ambraseys and Jackson,* 1997]. During the last 40 years the seismicity of the Corinth rift included six events of magnitude $M_s \geq 6$ (Eratini, 1965, M_s=6.4; Antikira, 1970, M_s=6.2; Corinth 1981, M_s=6.7, M_s=6.4, and M_s=6.2; Aigion, 1995, M_s=6.2). The focal mechanisms of all these earthquakes represent almost pure normal faulting with a N-S to NNW-SSE extension direction [*e.g., Baker et al.,* 1997] (Figure 1). Although the two main events of the 1981 sequence ruptured known 45-50° north dipping faults outcropping on the southern coast of the gulf [*Jackson et al.,* 1982; *Hubert et al.,* 1996], the 1995 Aigion earthquake ruptured a fairly low angle (33°) north dipping off shore normal fault not outcropping on land [*Bernard et al.,* 1997a]. This earthquake, together with the 1992 M_s=5.9 Galaxidi earthquake [*Hatzfeld et al.,* 1996], demonstrated that inner-rift normal faults could play an important role in the deformation of the rift and that these faults may have somewhat lower dips than the on shore ones. In addition, a 2-month microseismic study conducted in 1991 in the western part of the gulf [*Rigo et al.,* 1996], and covering the Aigion 1995 earthquake epicentral area, revealed a strong clustering of micro earthquakes. A significant number of these indicate north dipping, low-angle, normal-faulting focal mechanisms at 7-11 km depth beneath the northern coast of the gulf. This result suggested that the steeply north dipping normal faults seen at the surface root at these depths on a low-

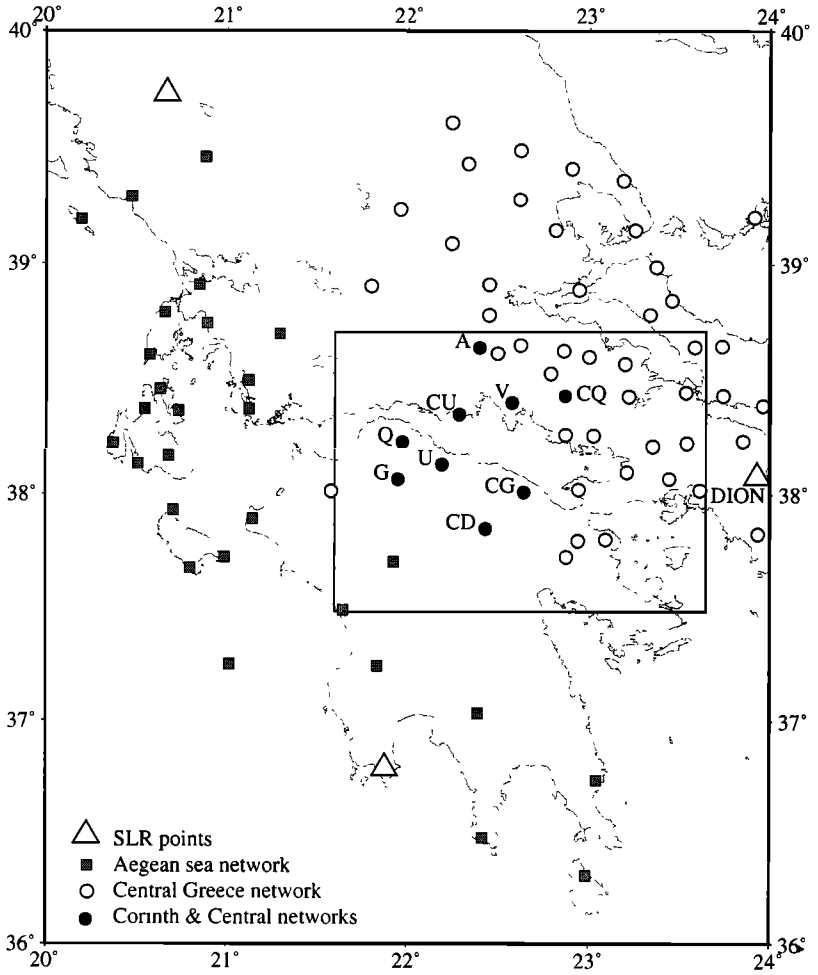

Figure 2. Geodetic networks in central Greece. Triangles are the satellite laser ranging (SLR) points. The SLR pad of Dionysos is used as reference for all GPS campaigns in central Greece. Shaded squares indicate the Ionian sea network [*Kahle et al.*, 1995]. Circles are the 66 points of the central Greece network [*Denys et al.*, 1994] installed in 1989. The eight solid circles, displayed with their code, are the central Greece points common with the Corinth rift network. Corresponding central Greece code can be found in Table A1 (available as electronic supporting material). The box indicates the location of Figure 3.

angle dipping (15° ± 10°) detachment zone [*Rigo et al.*, 1996; *Rietbrock et al.*, 1996].

Using the comparison between old triangulation observations and a GPS survey, *Billiris et al.* [1991] gave the first large-scale determination of geodetic deformation rate (10 mm/yr) and extension orientation (N-S) of the Corinth rift over a 100-year period. *Clarke et al.* [1997] give a more detailed picture of the deformation at the regional scale around the gulf based both on a 100-year comparison and on GPS results between 1991 and 1996. In particular, they show that the velocities increase smoothly from east (6.4 ± 1.0 mm/yr) to west (12.7 ± 1.0 mm/yr). They found that the geodetic velocity in the eastern gulf is in good agreement with that deduced by summing 100 years of energy released by earthquakes. This is not the case in the west, where the rate of seismic moment release predicts extension rates 2 to 3 times smaller than the lowest geodetic extension rate observed. According to *Ambraseys and Jackson* [1997] the frequency of large earthquakes in the eastern gulf during the period 1690-1890 has been higher than during this century, and they suggest that the deficit of seismic strain release in the western Corinth rift could be met by several such earthquakes in the medium term. However, the former comparisons of seismic and geodetic balances of energy release are strongly dependent on the effective thickness of the seismogenic layer.

On the basis of our dense geodetic data and on the knowledge gained from the 1995 Aigion earthquake, we will refine the extension rate across the rift and demonstrate that the deformation is strongly localized. We then study the consequences of this localization by means of simple dislocation models that allow us to discuss the inner/outer rift repartition of the deformation as well as the effective thickness of the seismogenic layer and the seismic/geodetic energy release.

2. Data

2.1. Geodetic Networks

During the last 10 years, several groups have installed and measured GPS networks in continental Greece at different spatial scales and in different areas (Figure 2). These networks are well tied together and have been colocated with the SLR pad of Dionysos during most of the GPS campaigns. In 1989 the "central Greece" network (66 points) covering an area of about 150 x 150 km was installed and measured by the National Technical University of Athens; the Universities of Newcastle, Nottingham, Oxford, and Cambridge; and the ETH Zurich for the purpose of monitoring the deformation of Central Greece at a large scale [*Denys et al.*, 1994; *Clarke et al.*, 1998]. Our network was progressively installed around the Gulf of Corinth starting in 1990, with the purpose of monitoring the deformation associated with the seismic cycle around the main active faults. It includes nine central Greece points. In October 1995 the network included 193 points. Among these, 51 are first-order points (Figure 3) observed during several long sessions (8 hours typically) in each campaign and with a precision of localization of a few millimeters, and 142 are second-order points increasing the density of the first-order network (Figure 3) but observed during short sessions (1-2 hours). The first-order network distribution has been established in order to ensure an accurate and pertinent determination of the deformation around the active faults where both spatial and temporal gradients of deformation are expected. Additional criteria such as accessibility, safety of the place, and local terrain stability have also been taken into account. This latter criterion has been difficult to satisfy along the southern coast of the gulf where most of the area is covered by young sediments and alluvial deposits (e.g., points D,T,Y,CI,CQ). In principle, the density of the second-order network (Figure 3) is high enough to ensure a sufficient number of displaced points for moderate earthquakes like the M_s=5.9 1992 Galaxidi and M_s=6.2 1995 Aigion ones. A network with such a spatial density was particularly useful for measuring the ground deformation associated with the June 15, 1995, Aigion earthquake and constraining the fault plane that ruptured during this event, the rupture size, and the amount of slip [*Bernard et al.*, 1997a]. All second-order points are pillars of the Hellenic triangulation network measured between 1966 and 1973. "Old" coordinates of these points have been recalculated in the Greek Geodetic Reference System (GGRS 87) [*Veis et al.*, 1992], and we present here a comparison of these coordinates with the GPS ones in addition to the comparison of GPS coordinates between 1990 and 1995.

2.2. GPS Campaigns

Overall, seven GPS campaigns took place in 1990, 1991, 1992, 1993, 1994, June 1995, and October 1995. Table 1 summarizes the characteristics of each campaign. During each campaign, the first-order points were measured in three or four sessions of 8 to 24 hours. The measurements were carried out using various types of Ashtech receivers (LD-XII, MD-XII, P-XII, Z-XII3).

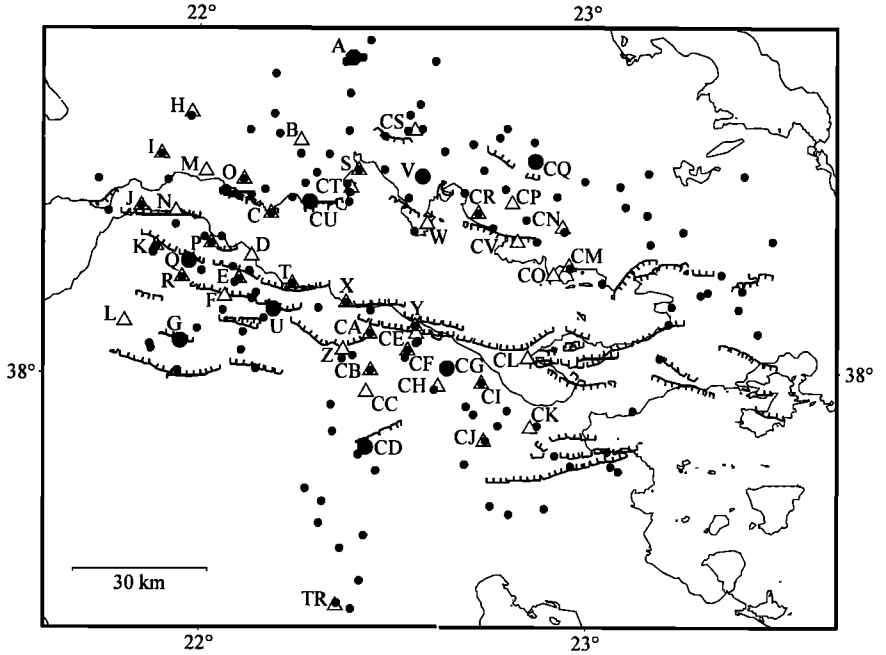

Figure 3. Corinth rift GPS network. The nine large solid points are common with the central Greece network. Triangles are the additional first-order points. Small points indicate the location of second-order points. All these points are pillars of the "old" Greek triangulation. Table A1 (electronic) displays coordinates and details about the first-order points, and Table A2 (electronic) displays coordinates and details about the pillars.

Table 1. Overview of the Seven GPS Campaigns

	1990	1991	1992	1993	1994	1995a	1995b
Starting date	May 8	Aug. 30	Nov. 27	May 10	Sept. 20	June 16	Oct. 3
Ending date	May 18	Sept. 10	Dec. 5	May 22	Oct. 2	June 24	Oct. 14
Number of codeless receivers	3	8	3	12	3	4	16
Number of code P-Z receivers				5	4	3	16
Number of permanent points			1	3	2	3	3
Number of first-order stations	7	23	9	43	16	23	51
Duration of one session, hours	4	6	4	8	8-12	12-18	8-24
Number of sessions per point	3	4	2-3	3-4	2-3	2-3	3-4
Ephemeris used for analysis	NGS	NGS	IGS	IGS	IGS	IGS	IGS
Software used for analysis	G	G-B	G	G-B	B	B	B
Vertical session to session scatter, mm	13	17	18	16	17	18	13
Horizontal session to session scatter, mm	3.5	3	4	4	4.5	4	4
rms in 3-D network adjustment, mm	10	12	8	9	14	13	9
Number of second-order stations		9		34	24	22	84
Duration of one session, hours		2		2-3	1-3	1-6	1-12
Number of session per point		1		1-2	1-2	1-3	1-3
Ephemeris used for analysis		b		b	b	b	b
Software used for analysis		G-A		A	A	B-A	B-A

G, GAMIT software; B, BERNESE software; A, Ashtech GPPS software; IGS, International GPS Service for Geodynamics; NGS, National Geodetic Survey (U.S.); b, broadcast orbits.

A few of the 1995 measurements were carried out using Leica and Trimble receivers. During the first campaigns, especially 1991 and 1993, most of the measurements were performed during evenings and nights to try to minimize both ionospheric and tropospheric effects. Later, because of the increasing number of receivers and decreasing number of operators, we often left the receivers unattended for longer periods of time, thus with day and night observations in the same data files at the same point. Starting in 1992, at least one station was maintained in permanent recording during the whole campaign. In the 1994 and 1995 campaigns, there were four permanent recording stations (Dionysos and points T, CH, and CT in the network).

2.3. GPS Data Processing

Processing of the GPS data was performed using GAMIT and BERNESE software for the first-order points and Ashtech Geodetic Post Processing Software (GPPS) software for the second-order points. Available data from the International GPS Service (IGS) stations Matera, Graz, Wettzell, and Madrid were included in the processing for the 1993, 1994, and 1995 campaigns. The coordinates of our network are expressed within the International Terrestrial Reference Frame 1992 (ITRF92) [*Boucher et al.*, 1993] for epoch April 1993. The reference point used for all campaigns was the main GPS point of Dionysos Observatory (DION) except for the first campaigns (1990 to 1992) in which DION was not measured. For those campaigns the reference has been arbitrarily fixed at point E. Owing to the small size of the network and the large deformations measured, this selection of a reference point at each campaign is purely technical, as errors as large as 20 cm in the absolute coordinates would not affect significantly the relative positioning. For the same reason, using the IGS stations as "fiducial" sites was not mandatory in our study. For the 1994 and 1995 campaigns we processed the IGS data together with the others, especially to improve the accuracy of vertical positioning. The relative horizontal coordinates within the network do not depend upon the introduction of IGS stations in the processing. For all campaigns we used the tropospheric parameters measured in the field (temperature, pressure, humidity) to fit the a priori model (the same tropospheric model of Saastamoinen is used by the GPPS, GAMIT, and BERNESE software) and let the software estimate an additional term of tropospheric delay correction in windows of 6 hours. For the second-order points the Ashtech GPPS software does not estimate an additional term of tropospheric delay, and the data were processed by introducing one unique set of tropospheric parameters for the whole session. The data from the later campaigns are fairly good, especially those obtained from Z-code Ashtech receivers. In contrast, some 1990-1991 data were difficult to clean for cycle slips because of the lower signal/noise ratio of the first generations of receivers and the higher level of solar activity in early 1990s inducing high ionospheric perturbations. Because of the moderate size of the network we were able to fix almost all phase ambiguities for all campaigns. The accuracy of the solutions is summarized in Table 1. For each campaign we tested the quality of our processing according to two criteria:

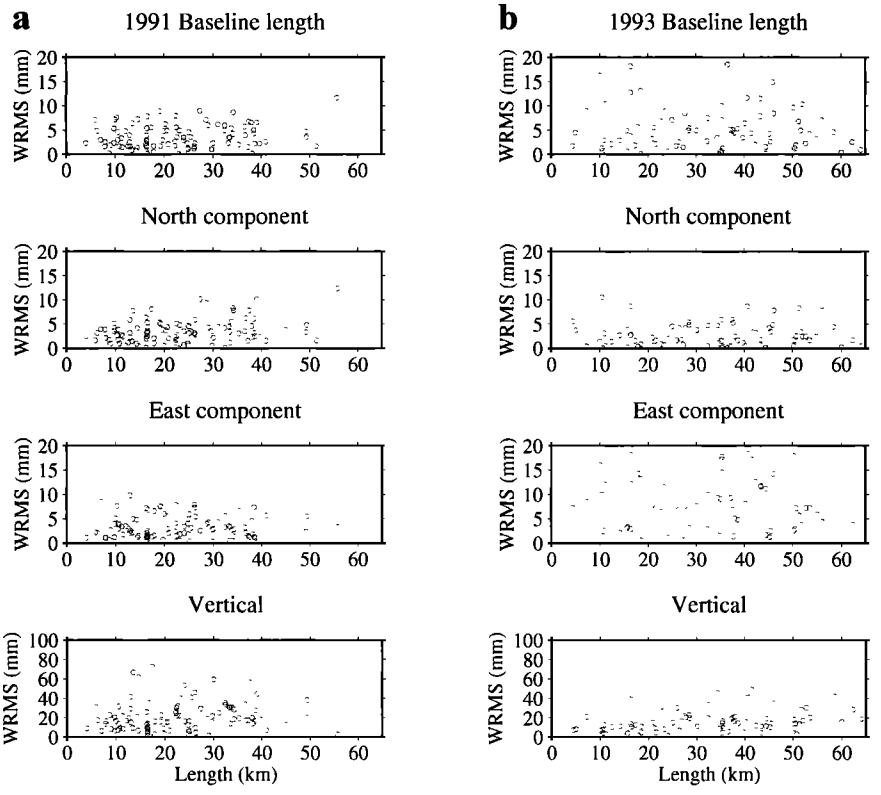

Figure 4. Session to session scatter versus baseline length for (a) the 1991 and (b) the 1993 GPS surveys. For each day the data were processed with the GAMIT software using precise orbits (NGS orbits in 1991 and IGS orbits in 1993). Each GPS station was occupied during four sessions of about 8 hours. Several baselines have been measured two, three, or four times. The plotted circles are the weighted rms deviation from the weighted mean of different components (length, north, east, and vertical) of these baselines. The average rms for all the baselines are reported in Table 1. For the baseline length the average rms is 3 mm for the 1991 campaign and 4 mm for the 1993 campaign.

1. We checked the day-to-day repeatability of the baselines (for the baselines measured at least two times). In Figure 4 we show for example the root-mean-square (rms) scatters in east, north, and up components and in distance versus baseline length for the 1991 and 1993 campaigns. All the campaigns were analyzed in the same manner and the baseline repeatability of each of them is given in Table 1. The horizontal repeatability is ~3-4 mm, and the vertical one is between 1 and 2 cm. Also, there is no correlation between the length of the baseline and the quality of the repeatability (Figure 4), the repeatability of a given baseline being more dependent on the difference in elevation between the points than on the length of the baseline itself. This is related to nonmodeled tropospheric effects.

2. For each campaign the coordinates were adjusted to fit the baselines using a least squares adjustment technique [*Tarantola and Valette,* 1982], in a code (AG3D) developed at Institut de Physique du Globe de Paris (IPGP) [*Ruegg and Bougault,* 1992]. The rms of the residuals after adjustment gave us another estimate of the global consistency of the network. For all the campaigns, there is a good agreement between the average scatter of the individual baselines before adjustment and the rms of the global adjustment (Table 1).

3. Results

3.1. Basic Results and Their Implications

Figure 5 shows the 1991-1993 displacements in the western Gulf of Corinth where measurements started in 1990 and 1991. It clearly indicates that, over the 3 years sampled, most of the deformation occurs off shore in the central part of the rift. The extension occurs on average along an axis oriented N9°E, consistent with the regional tectonics.

Figure 6 displays the time series of 1990-1995 relative displacements (values in Table 2) of line A-G, projected along the N9°E axis. At the first-order and according to the error bars on the coordinates at each epoch of observations, the extension of the rift is a linear function of the elapsed time between 1990 and 1994. The southern side of the gulf appears to behave as an almost rigid block. The northern side of the gulf, between points B and A appears also to behave as a rigid block, whereas

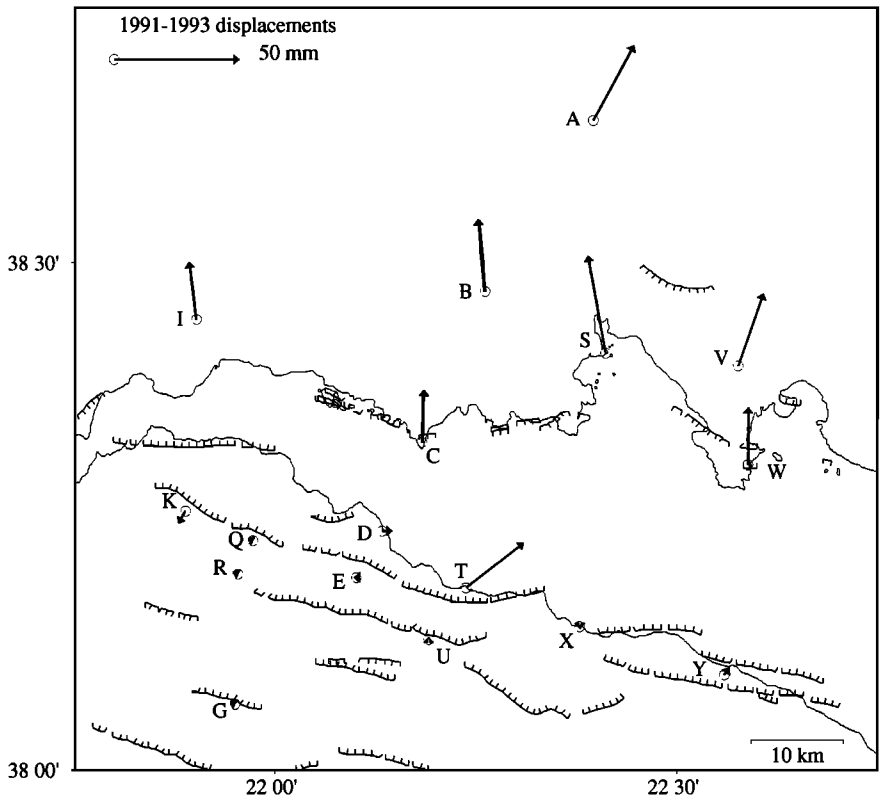

Figure 5. The 1991-1993 displacements in the western part of the Corinth rift; G is fixed.

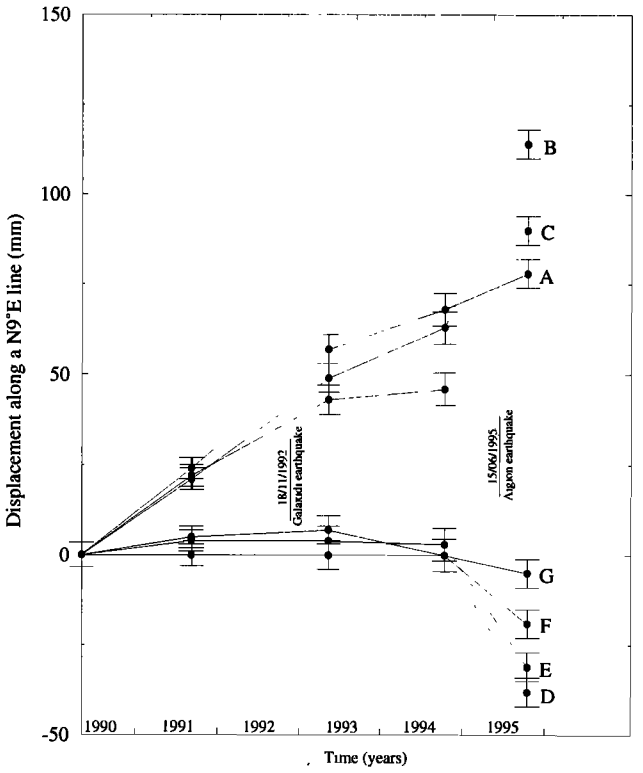

Figure 6. N9°E projection of the displacements (mm) of points A,B,C,D,E,F,G as a function of time. Error bars for each individual campaign are drawn. The change in the slope of the curves between 1994 and 1995 corresponds to the coseismic displacements associated with the June 15, 1995, Aigion earthquake. Points A and G are not sensitive to that earthquake.

the extension rate at point C is somewhat lower than at B and A. This trend changes between 1994 and 1995 owing to the M_s=6.2, June 15, 1995, earthquake. Between 1993 and 1994 the data suggest that the extension rate of the northern side might have been lower than during the previous years, but the change is subtle except at point C. We estimate that the hypothesis of a change of extension rate before the 1995 earthquake is not sufficiently supported by our data to be discussed here.

In this paper, we use these raw results to present a more refined analysis.

1. From the results of Figure 6, we argue that at the first order, over short periods of time, the deformation of the rift is the sum of a linear deformation field and of the contribution of the earthquakes.

2. We use this argument to separate in our geodetic data the contribution of the 1992 and 1995 earthquakes from the total observed deformation.

3. We use the relative rigidity of the southern and northern blocks to scale and rotate coordinates issued from classical geodetic observations within the GPS coordinates frame.

3.2. Coseismic Deformation

Two significant earthquakes occurred during the period of our surveys, on November 18, 1992 (M_s=5.9, Galaxidi), and on June 15, 1995 (M_s=6.2, Aigion). Coseismic displacements were measured at six points for the 1992 earthquake (C, D, S, T, X, V) (Plate 1a) and at 29 points for the 1995 one (Plate 1b). We also cal-

Table 2. Horizontal Displacements of Points A to G as a Function of Time

Year	Months	A	B	C	D	E	F	G
1991	16	24	21	22	5	4	0	0
1993	36	57	49	43	7	4	0	0
1994	53	68	63	46	0	3	0	0
1995	65	78	114	90	-38	-31	-19	-5

Displacements are in mm. The number of months refers to the date of the first campaign (May 1990).

culated ERS synthetic aperture radar (SAR) interferograms for time intervals covering both earthquakes. We used the velocity field deduced from Figure 5 to correct our measurements for the long-term motion and to properly extract the coseismic contribution. The displacements associated with the June 15, 1995, earthquake are relatively large (up to 10 cm) and above the level of noise at more than 20 points. These data were used together with SAR interferometry (InSAR) and seismological data to constrain a dislocation model [*Bernard et al.*, 1997a]. Compared to the model proposed by *Bernard et al.* [1997a], the model presented here (Plate 1b and Table 3) takes into account a few additional GPS vectors, but there are no significant differences in the parameters of both models. The displacements associated with the November 18, 1992, earthquake are small ($\leq$ 20 mm). Plate 1a displays the coseismic data for the 1992 earthquake and a dislocation model assuming a north dipping plane located at the eastern end of the 1995 fault. A preliminary analysis (based on displacements observed at points C, X, S, T, U, V) proposed that the 60° south dipping plane was the fault plane [*Briole et al.*, 1993] but further seimological analysis [*Hatzfeld et al.*, 1996] indicated that a 30° north dipping plane, as for the 1995 Aigion earthquake [*Bernard et al.*, 1997a], is the most probable solution. Also the InSAR data agree better with this interpretation: the synthetic interferogram calculated assuming a north dipping plane (Plate 1c) exhibits no fringes in the northern coast of the gulf, as it is the case in the data. In contrast, the synthetic interferogram calculated assuming the antithetic south dipping fault plane (Plate 1d) exhibits two fringes above the northwestern edge of the fault. In this case, to obtain a synthetic interferogram without fringes, it is necessary to shift the fault plane 3 km to the south, inducing a displacement at point S not compatible with the observations any more. There is no way of fitting both the GPS data and the InSAR data if one assumes a south dipping plane for the 1992 earthquake. The parameters of both the 1992 and 1995 dislocation models are given in Table 3 together with the parameters of the other earthquakes of magnitude $M_s \geq 5.5$ that occurred since 1965. The coseismic contribution of all the earthquakes (except the 1965 event, which occurred before the first triangulation measurement) has also been calculated and is discussed in section 3.4.

3.3. Continuous Deformation on the First-Order Network

Figure 7 displays the velocity vectors in the Corinth rift after removing the coseismic contributions of the 1992 Galaxidi and 1995 Aigion earthquakes. The values are listed in Table A1 in the electronic supporting material[1]. To bring the coordinates issued from the processing of each campaign into the same reference frame, we have considered the Peloponnisos as a fixed reference. For the period 1990-1994, all Peloponnisos points except points X and T that were affected by the 1992 earthquake have been used to minimize the residual displacement vectors between epochs. For the comparison of the 1995 campaigns with the previous ones, points P, Q, R, D, E, F, U, and T close to the 1995 earthquake have been discarded and the Peloponnisos points used for minimization were K, L, G, and all points located southeast of point X (see Figure 3). No long-term velocity has been calculated for points S and T that are affected by both earthquakes. Figure 7 also displays the velocities obtained over 100 years by comparing recent GPS coordinates with coordinates obtained from triangulation fieldwork carried out in 1892 [*Davies et al.*, 1997], the velocities obtained by *Kahle et al.* [1995] over the Ionian sea network and the velocities obtained by *Anzidei et al.* [1996] at CHLE point (west Peloponnisos). With respect to the deformation located in the inner Gulf of Corinth, little internal deformation occurs in Peloponnisos, even along its northern coast. This result is consistent with the other geodetic studies carried out at a broader scale [*Billiris et al.*, 1991; *Davies et al.*, 1997; *Clarke et al.*, 1998; *Kahle et al.*, 1995; *Veis et al.*, 1992], and its originality lies in the higher number of points that allows a better constraint on the width of the deforming zone. Most of the deformation occurs offshore between the southern and the northern coasts of the gulf. North of the Gulf of Corinth, the vectors are almost parallel to each other in the central and western areas but rotate in the northeastern region from N10°E to N30°W, so they remain almost perpendicular to the tectonic structures there (Kaparelli fault zone). In this area, deformation associated with the progressive change of orientation of the extension is probably occurring. However, the sampling interval of only 2 years in the east (1993-1995) limits

[1]Supporting data Tables A1 and A2 are available on diskette or via Anonymous FTP from kosmos.agu.org, directory APEND (Username=anonymous, Password=guest). Diskette may be ordered from American Geophysical Union, 2000 Florida Avenue, N.W., Washington, DC 20009 or by phone at 800-966-2481; 15.00. Payment must accompany order.

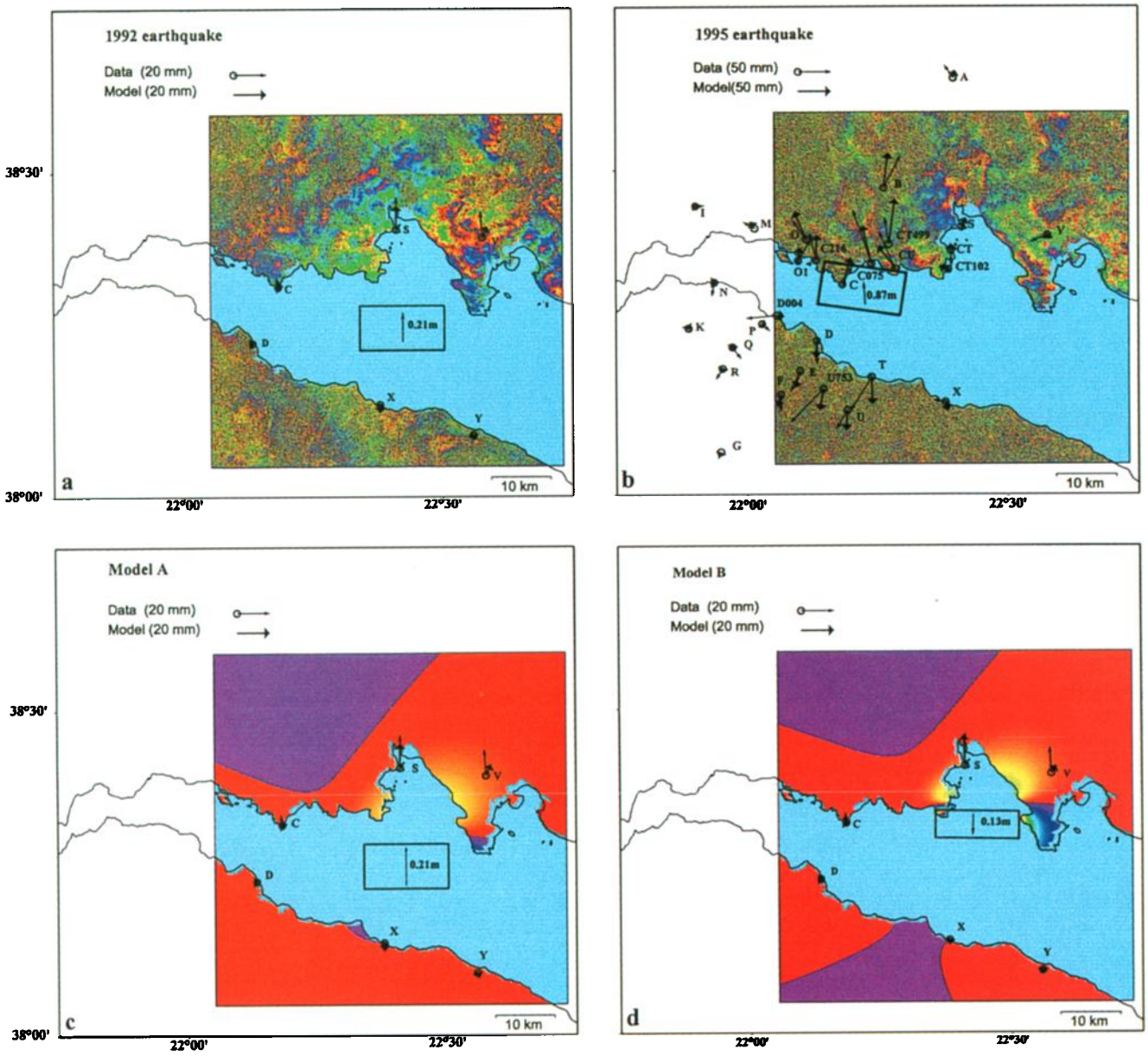

Plate 1. (a) Observed and modeled coseismic displacements associated with the November 18, 1992, Galaxidi earthquake. Projection of the fault at the surface is shown with the slip vector. Parameters of the model are given in Table 3. Also plotted is the interferogram obtained using the pair of images ERS1 5162 (July 11, 1992) and ERS1 10172 (June 26, 1993) with altitude of ambiguity of 603 m. Note that no fringes are visible. (b) Observed and modeled coseismic displacements associated with the June 15, 1995, Aigion earthquake. Projection of the fault at the surface is shown with the slip vector. Parameters of the model are given in Table 3. Also plotted is the interferogram obtained using the pair of images ERS1 6164 (September 19, 1992) and ERS1 22039 (October 2, 1995) with altitude of ambiguity of 972 m. Note that this interferogram is almost identical to that shown by *Bernard et al.* [1997a] that was calculated over a period of 4 months only. (c) Modeling of November 18, 1992, Galaxidi earthquake and predicted interferogram for a 30° north dipping plane of length 14 km and width 9 km. No fringes are predicted by this model (model A). (d) Model B corresponds to a 60° south dipping fault plane of same area as model A and predicts two fringes on the northern coast.

Table 3. Parameters of the Recent Earthquakes in the Gulf of Corinth

Event	M_0, 10^{18} N m	Longitude, °E	Latitude, °N	Strike, deg	Dip, deg	Rake, deg	Length, km	Width, km	Centroid, km	Slip, m
July 6, 1965 [a]	1.7	22.40	38.37	281	34	-72	13.	8.	10.	0.5
April 8, 1970 [a]	0.9	22.56	38.34	265	23	-81	12.	7.	9.	0.32
Feb. 24, 1981 [b]	8.8	22.97	38.23	264	42	-80	18.	14.	12.	1.07
Feb. 25, 1981 [b]	4.	23.12	38.17	241	44	-85	16.	14.	8.	0.54
March 4, 1981 [b]	2.7	23.26	38.24	50	45	-90	12.	14.	7.	0.49
Nov. 18, 1992 [c]	0.9	22.45	38.30	270	30	-81	14.	9.	7.4	0.21
June 15, 1995 [d]	3.6	22.20	38.36	277	35	-81	14.	9.	7.1	0.87

The coordinates refer to the projection at the surface of the center of the upper edge of the fault.

[a] *Baker et al.* [1997].

[b] *Taymaz et al.* [1991].

[c] Revised from *Hatzfeld et al.* [1996] and *Briole et al.* [1993]. Both studies indicate that the surface of the ruptured plane is rather large for an earthquake of this magnitude. The seismic moment found by the waveform modeling is 0.4 x 10^{18} N m, the Harward centroid moment tensor (CMT) is 0.5 x 10^{18} N m and the seismic moment deduced from the inversion of the geodetic data is 0.9 x 10^{18} N m.

[d] *Bernard et al.* [1997a] modified to take into account a few additional GPS data. The seismic moment for this earthquake is deduced from the modeling of the GPS and SAR data. It is 5% higher than the seismic moment deduced from the waveform modeling (3.4 x 10^{18} N m) and 30% lower than the revised Harward CMT (5.1 x 10^{18} N m).

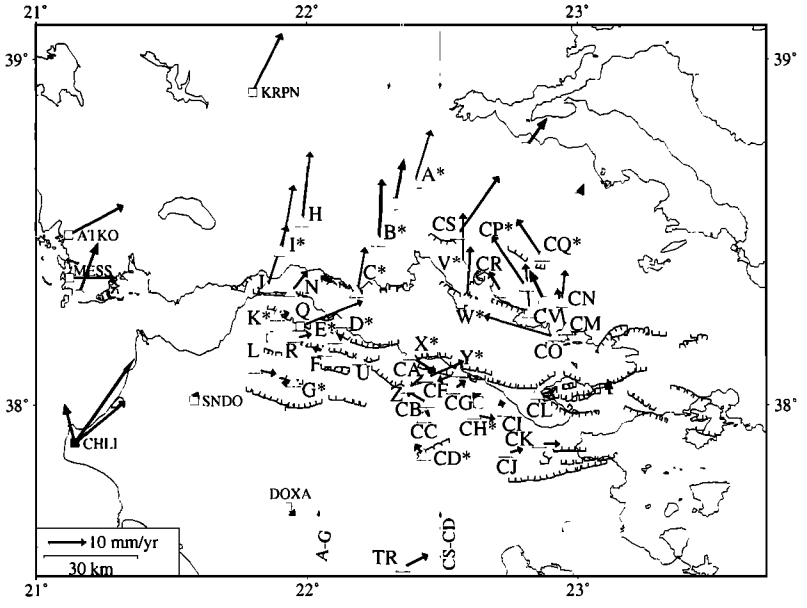

Figure 7. Relative velocities of GPS points across the Corinth rift. The 1990-1995 velocities of 41 first-order points of the Corinth rift network are shown, with Peloponnisos fixed (obtained by minimization of the residual of the velocity vectors of all points located south of the gulf). Points with star have been measured during three or more campaigns. The velocities obtained in other studies are also plotted: 1989-1993 velocities on the Ionian sea network [*Kahle et al.*, 1995], of particular interest at points KRPN, Q, SNDO, and DOXA that complete our network to the west; the thicker arrows are 1892-1992 velocity vectors [*Davies et al.*, 1997] at four locations to the north of the gulf (one between points A and B, one between points CV and CN, and two north of CQ), one location in the east (east of CL), and three locations to the south of the gulf (one south of CK, one at CG, and one between K and L). There is, in general, a good agreement between the determinations of the other groups and our velocity vectors, except at point Q, where the result of *Kahle et al.* [1995] is not consistent with our determination and with the general observation that the Peloponnisos has not internally deformed over the observed interval. At point CHLE the three vectors show three different determinations of the velocity of the points, with reference to Peloponnisos fixed, two determinations being from the above references, the last one (thin arrow) given by *Anzidei et al.* [1996]. Profiles A-G and CS-CD used in the further discussion are drawn.

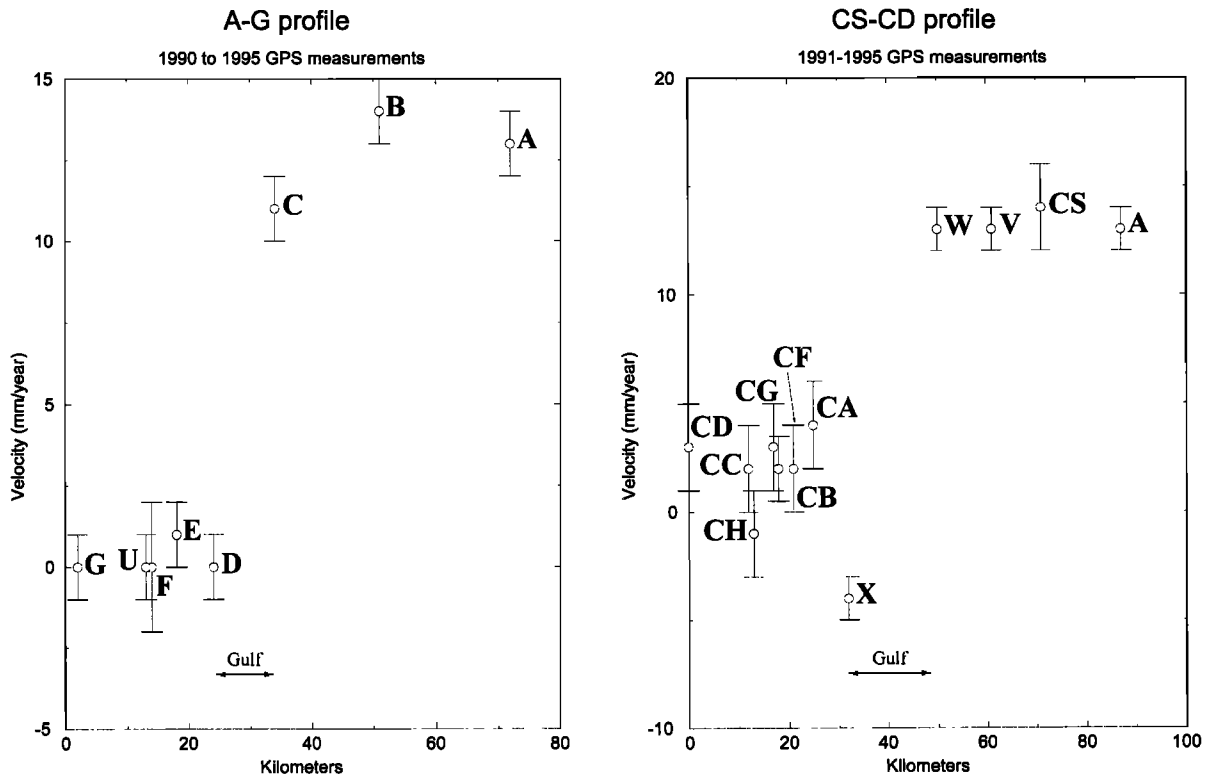

Figure 8. The 1990-1995 GPS velocity along profiles A-G and CS-CD (all points located closest than 12 km to the profile have been included) and error bars. The extension rate is 14 mm/yr along line A-G in a N9°E azimuth and 13 mm/yr along line CS-CD in a north azimuth.

the accuracy. Figure 8 shows the projection of the velocity vectors plotted in Figure 7 along two lines (A-G and CS-CD) crossing the rift at two different locations, and sampling two of the main structures discussed in section 5, the Helike fault (line A-G) and the Derveni-Xilokastro fault (line CS-CD). These sections indicate extension rates and azimuths of 14 ± 2 mm/yr along line A-G in a N9°E direction and 13 ± 3 mm/yr along line CS-CD oriented N-S. These values of extension are in relatively good agreement with the results of *Clarke et al.* [1997] but are somewhat lower, in particular in the western part of the gulf, where we do not measure extensions higher than 15 mm/yr while Clarke et al. find values up to 20 mm/yr. The only areas where gradients of deformation are observed on land are around point C (northern side) and to the west of point C as mentioned by *Bernard et al.* [1997b] and *Clarke et al.* [1998] and around points J and N (southern side). The maximum width of the deforming area has thus an upper bound equal to the width of the gulf, that is 10 km on the H-L line, 15 km on the A-G line, and 30 km on the two eastern lines. Its lower bound seems to be of the order of 10 km as suggested by the observed offshore gradients of deformation. Figure 7 suggests that internal deformation is occurring in the eastern part of the northern block, in particular, in the area located between CR, V (Antikira area), CQ, and CS. Inside this area (Livadia-Arakhova) the orientation of the velocity vector changes in a relatively narrow band from a N30°W to a N-N30°E direction. Figure 7 also indicates that the orientation of the velocity vector at CS is consistent with the orientation of the two velocity vectors computed for the time interval of 100 years on the two points located south of the Evvia Gulf. This result has to be confirmed by additional measurements over a longer period.

3.4. Continuous Deformation of the Second-Order Network

The second-order GPS network consists of pillars previously measured by classical means during campaigns carried out between 1966 and 1973. Because we did not try to occupy remote points located on the highest mountains, most of these pillars are third- or fourth-order triangulation. The 1966-1973 coordinates of those points were computed as a single epoch network by forcing it to conform with the first- and second-order triangulation carried out in 1974. The average standard error (1σ) for the positions of these third- and fourth-order points were calculated to be of the order of 3 cm [*Veis et al.*, 1992]. For the entire country of Greece the 25,000 coordinates calculated for this epoch of measurement (early 1970 on average) constitute the "Greek Geodetic Reference System 1987" (GGRS-87) [*Veis et*

Table 4. Rotation and Scale Correction of the Triangulation Data

Area	Points	Rotation, ppm	Scale, ppm	rms S, mm	rms N, mm
South	69	4.25	2.3	125	164
North	61	6.1	2.55	154	146
Average		5.2	2.4	133	150

Rotation and scale adjustment of the triangulation coordinates to the GPS coordinates have been calculated assuming no internal deformation of both southern and northern block. The rms scatter between the two sets of coordinates is displayed after correction is applied. Two estimations have been done: one with the northern side rigid (61 points), and one with the southern side rigid (69 points). Under both assumptions, the rms have been calculated separately for both sides of the gulf. Rigid north side assumption leads to rms values slightly higher. Scale correction is almost the same for both estimations: the difference of 0.25 ppm corresponds to an error of 25 mm at a distance of 100 km, which is well below the best residual rms (125 mm). The range of possible rotation parameters (1.85 ppm) leads to maximum changes of 185 mm at 100 km that is comparable with the residual error level. Assuming that the errors in the second epoch of observations (GPS) are negligible and provided that the uncorrected tectonic motions have no reason to be correlated with the measurement errors, 125 mm is a measure of the maximum statistic error on the triangulation coordinates (including both measurement and processing errors). Indeed, a detailed analysis of the residual vectors between close points in the southern block shows that the errors in the triangulation coordinates are more likely to be of the order of 50 mm, that is, roughly consistent with the value of 20-30 mm given by *Veis et al.* [1992].

al., 1992]. They are given to an accuracy of a few centimeters plus one part in 10^6, while the scale and orientation are on average within a few parts of 10^{-7} of the internationally accepted reference system ITRF89 [*Boucher and Altamimi,* 1989; *Boucher et al.,* 1993]. We measured a total of 159 triangulation pillars (Table A2, electronic), 17 belonging also to the first-order GPS network. We were able to compare the coordinates for 146 of them (in some cases, the comparison indicated that the pillars had been displaced and in few cases, the old coordinates were not available). We neglected the duration of each series of campaigns (7 years for the first one that occurred between 1966 and 1973 and 4 years for the GPS campaigns) with respect to the mean time interval of 24 years between the two series of campaigns. This approximation is justified by the a priori size of the errors associated with the triangulation measurements and further validated by the standard error deduced from our study (Table 4). We divided the pillars into four categories based on their location: 69 in the south of the gulf, 61 in the north, 14 in the east, and 2 in the west. The direct comparison of the 1991-1995 GPS coordinates and the 1966-1973 coordinates is represented in Figure 9a. Point E, near Aigion, is arbitrarily kept fixed for the comparison of the two sets of data, although any other point could have been kept fixed. The general trend of the raw displacement vectors in the northeast and in the southeast does not agree with the results of the GPS-GPS comparisons presented in section 3.3 (Figure 7) and indicates that a correction for orientation and scale should be applied for the old coordinates. On the basis of the precision of the old data, we limited the correction for the old coordinates to a two-parameter correction (scale and orientation), an approximation further validated by the results obtained on the corrected coordinates of pillars. To find the best values for scale and orientation correction, we minimized the displacement vectors of the 69 points located in Peloponnisos, according to the observation from the repeated GPS surveys that this block is not significantly deforming with respect to the inner gulf zone. The best fit was found with a counterclockwise rotation of 4.25 ppm and dilatation of 2.3 ppm. Those values of scale and rotation are somewhat higher than were predicted at the regional scale from the adjustment of the triangulation data [*Veis et al.,* 1992]. This suggests that there could be locally some bias higher than the global average, due to nonhomogenous networks (offshore areas) and problems of connections between networks measured during different field campaigns. Assuming the northern block of the Gulf of Corinth to be rigid (61 points), the minimization leads to values of +6.1 ppm for the rotation and +2.5 ppm for the scale. The most important fact is the similarity of the values found for the scale correction, the difference between the two determinations being below the value of the errors on the determination itself. In Table 4 we summarize the values of the rms found on both sides of the gulf for the above two sets of rotation and scale factors and for an intermediate value. As the scatter between both solutions remains below the errors on the pillar coordinates determination, in the following, we adopt the values of +4.25 ppm and +2.3 ppm for the orientation and scale correction; these are the values that give the best fit for the 69 points located in Peloponnisos. The amplitude of coseismic displacements estimated over 24 years from the parameters in Table 3 (Figure 10) is much less than the extension measured geodetically over the same period, except possibly in the Alkyonides area where a relatively large part of the deformation could be explained by the 1981 earthquakes [*Rigo,* 1994]. Figure 11 shows the projection of the vectors plotted on Figure 9, along the lines A-G and CD-CS (see Figure 7) used for projecting the GPS velocities and along an additional line crossing the Thivai area at the eastern end of the gulf. The high rates found from the comparison GPS triangulation are not compatible with the GPS-GPS estimation of velocities in the Gulf of Corinth. On lines A-G and CS-CD, the average overestimation of the velocities is 80% with respect to the GPS-GPS ones. This overestimation of the velocities across the Corinth rift could be due to errors in con-

necting classical geodetic data from one to the other side of the gulf. Indeed, although the old coordinates are correctly scaled at the global scale, as indicated by *Veis et al.* [1992], they could present distortions at the intermediate scale due to the nonhomogeneity of the network and to the fact that the third- and fourth-order networks were measured during several field campaigns, implying possible problems of connection between each survey during the adjustment phase.

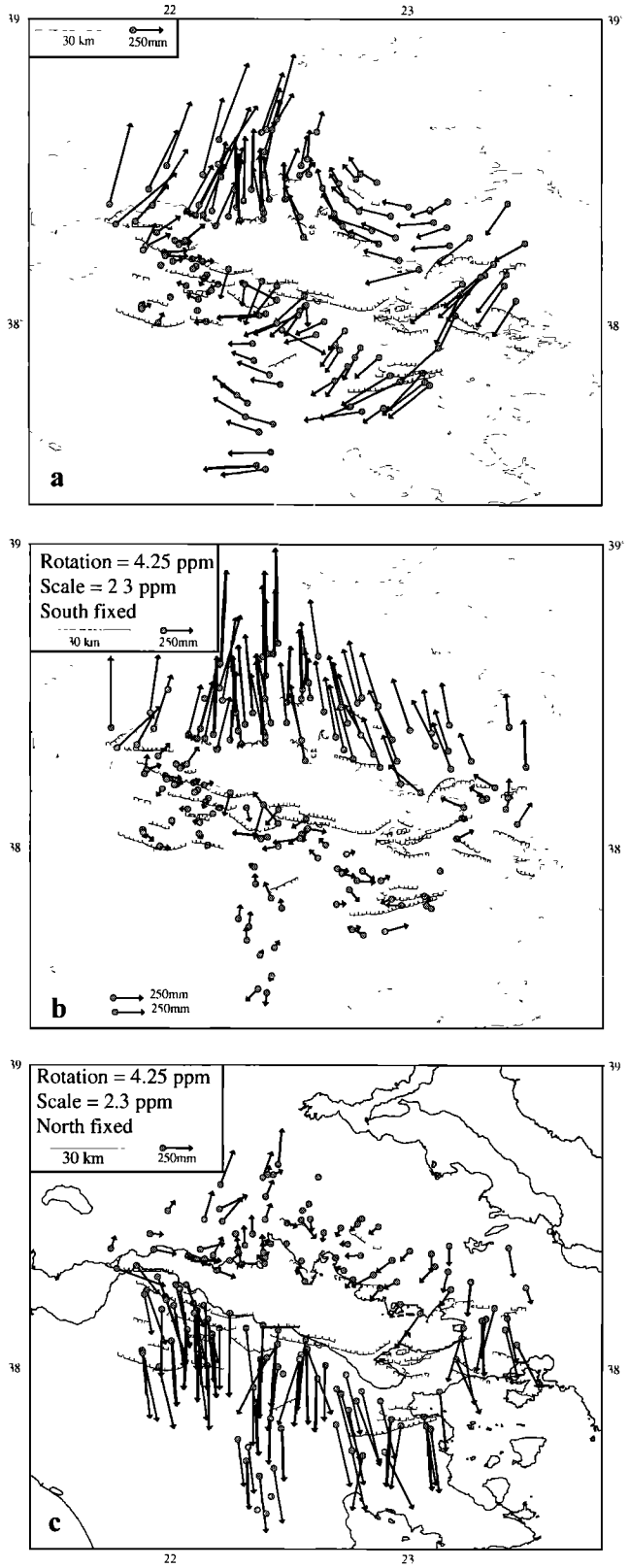

Figure 9. (a) Comparison of the 1991-1995 GPS coordinates of 146 pillars of the Hellenic triangulation network with their 1966-1972 coordinates obtained from terrestrial measurements. First-order point E is used as common reference for comparison of the two epochs. (b) Displacement of the 146 pillars after counter clockwise rotation of +4.25 ppm and dilatation of +2.3 ppm that minimizes the residuals on the 69 pillars located in the southern part of the gulf. The barycenter of the 69 pillars is used as common reference for comparison of the two epochs (the sum of the displacement vectors of the 69 points equals 0). (c) Same displacement field as in Figure 9b but with the barycenter of the 61 pillars located north of the gulf kept fixed.

3.5. Summary of the Observations

The main results of the data analysis are as follows:

1. The extension rate measured over 5 years across the Corinth rift ranges between 15 and 10 mm/yr from west to east. The extension rate measured over 24 years by comparing GPS and triangulation coordinates overestimates the above values by 50 to 80%, probably due to distortion in the triangulation data at the regional scale due to both spatial inhomogeneity of the data (presence of the sea) and temporal inhomogeneity of the data (several field campaigns between 1966 and 1973).

2. Both data sets indicate that the southern side of the gulf behaves like a rigid block. On the northern side, there is a regional east-west compression and local gradients of deformation at points located near the northern coast, west of point C.

3. In consequence, almost all the deformation is localized offshore, within the inner part of the Corinth rift. The deformation is particularly localized (~10 km width) in the western part of the rift (Aigion-Psathopirgos). The localization is less well defined in the center of the rift (Derveni, Xilokastro), where the gulf is wider. The deformation seems to be more diffuse in the eastern part of the rift (Corinth, Thivai). The largest opening rate (14 mm/yr) is measured at the longitude of Aigion, where the width of the deforming zone is apparently the lowest. The implications of such a localization are very important and are discussed in section 4.

4. No movement is observed across the active faults bordering the southern coast of the gulf like the Helike and the Xilokastro faults. These faults thus appear to behave in a locked-seismic mode.

5. The extension direction (Peloponnisos assumed fixed) rotates from about N9°E in the west to about N20°W in the east of the rift, in relatively good agreement with the focal mechanisms of earthquakes and the orientation of the active faults observed in the field.

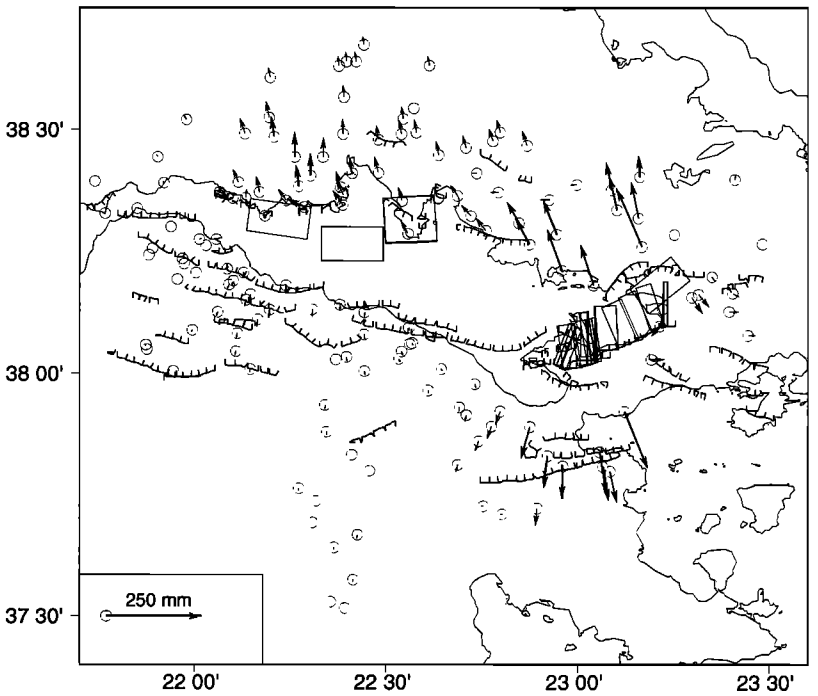

Figure 10. Modeled coseismic displacements associated with all earthquakes of magnitude ≥ 5.5 that occurred within the network between 1966 and 1995. The parameters of the modeled faults are those of Table 3. The area where displacements could be observed given the accuracy of the old measurements (50 to 125 mm) is limited. The amplitude of the predicted displacements is much lower than that of the observed motions.

4. Deformation Modeling

In order to interpret our observations we construct a model based on the simple assumption of deformation in an elastic half-space. We make the hypothesis that the deformation is localized along active faults or in relatively narrow deforming zones for which a planar fault model is a good approximation to predict deformation in the near and far field. This hypothesis has been discussed by *Gilbert et al.* [1994] in the case of the San Andreas fault and is also supported by numerical modeling of extending areas [*Hassani and Chéry,* 1996]. The geometry of the faults that enter our model is controlled by available tectonic and seismological information. The study of uplifted marine terraces in the Xilokastro as well as the Derveni and Aigion areas [*Rigo,* 1994; *Armijo et al.,* 1996] gives estimates of slip rates on the main faults bordering the southern coast of the gulf. *Armijo et al.* [1996] estimated a long-term slip rate on the Xilokastro fault of 11 ± 3 mm/yr on a 50° dipping plane. On the other hand, the analysis of the June 15, 1995, Aigion earthquake [*Bernard et al.,* 1997a] pointed out the importance of the inner-rift active low-dipping faults in the process of extension of the Corinth rift. The inner-rift activity is further corroborated by the smaller M_s=5.9 Galaxidi earthquake [*Hatzfeld et al.,* 1996] that occurred on a ~30° north dipping fault. The 1965 and 1970 earthquakes that occurred close to the northern coast of the gulf with similar mechanisms as the Aigion and Galaxidi events (Figure 1) are also good candidates for inner-rift activity on a shallow north dipping plane, although no constraints are available on the rupture plane for these events. In addition, the observed deformation presented here occurs mostly offshore. As we will see below, this observation cannot be explained with faults located only along the southern coast of the gulf. We thus impose the geometry shown in Figure 12 where the two systems of faults (F5 for outer and F1 and F2 for inner rift) are assumed to join at depth at the brittle-ductile transition zone represented as a gently north dipping decollement surface (F3 and F4) as proposed by *Rigo et al.* [1996] and also supported by the multiplet analysis of *Rietbrock et al.* [1996]. We assume that the extension is driving creep on this decollement (F3) that we model as continuous slip. F2 and F5 are assumed to be seismic faults, locked during the interseismic period and slipping during earthquakes. Characteristic earthquakes for F2 and F5 are the M_s=6.2 Aigion and the M_s=6.6 Helike earthquakes, respectively. Either continuous or locked-seismic slipping modes can be assumed for F1 and F4. At each fault junction (F1-F2 and F4-F5) the amplitude of horizontal motion is assumed to be continuous. At the F2-F3-F4 triple junction the kinematic compatibility for horizontal motion is assumed. These conditions allow us to calculate slip rates on each fault, given that v_3, the slip rate on F3, is deduced directly from the data and assuming a given partitioning of the opening between the inner and the southern

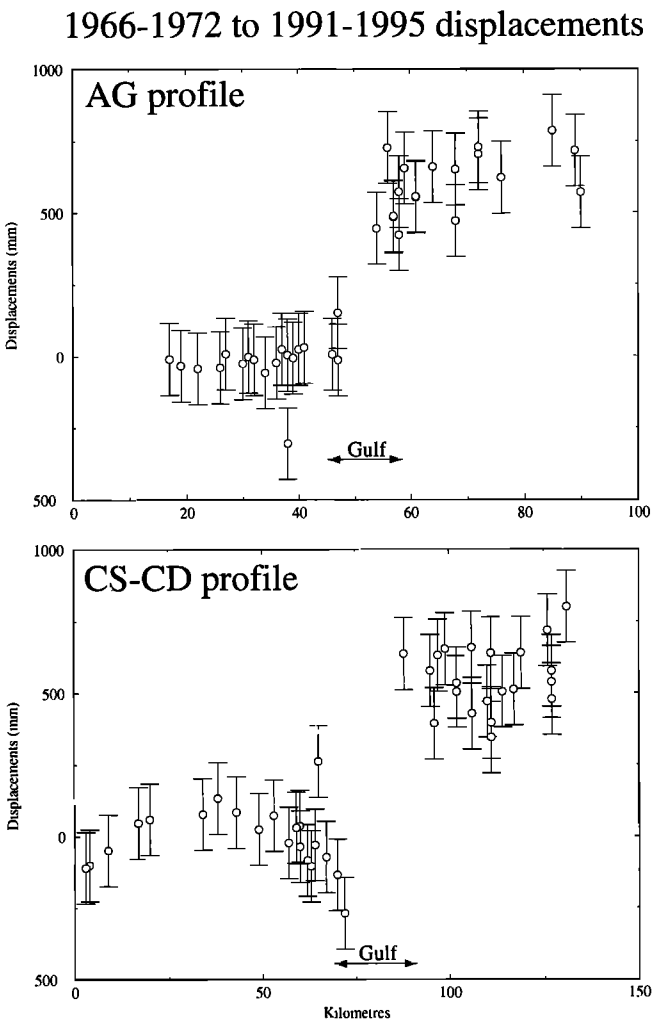

Figure 11. Displacement profiles obtained from the triangulation GPS comparison along profiles A-G and CS-CD over an average period of 24 years. On A-G the average opening between the two sides of the gulf is 600 mm, which corresponds to a rate of 25 mm/yr. On CS-CD the average opening is 534 mm or 22 mm/yr.

faults. We use these slip rates to compute the deformation induced by the continuous slipping segments as well as the predicted seismic energy release and recurrence time of earthquakes on the seismic faults. We also tested models where slip is continuous from F1 to F2 and from F4 to F5. This type of model did not yield significantly different results, and here we discuss only models based on the continuity of horizontal motion, which seems more realistic.

We first ran a series of tests to demonstrate the impossibility for fault F1 to behave in a locked-seismic mode. For this test we assume continuous slip on F3-F4 only, for three variable depths of these faults (corresponding to 8, 6, and 4 km for the F5-F4 junction). The predicted rates of opening are compared to the observations for profile A-G in Figure 13. None of the three models fits the highly localized observed opening zone, and the only way to localize this deformation is to assume some continuous deformation at shallow level in the uppercrust beneath the gulf. We choose to confine this continuous deformation to the upper 2.5 km and to model it as continuous slip on F1. This does not mean we believe F1 really slips continuously. Rather, we think that the uppermost few kilometers of the crust, which include thick sediments in the gulf, are deforming by creep. This has been suggested for the western United States [*King et al.*, 1994], partly on the basis of the absence of seismicity at shallow depths which we find here also [*Rigo et al.*, 1996; *Bernard et al.*, 1997a]. Whether this creep is localized on one fault as assumed here, or on a few faults, or is distributed in volume, cannot be resolved from our data and thus is not relevant for the modeling presented here.

4.1. Aigion Profile (Line A-G)

The opening rate deduced from the GPS data is 14 mm/yr. Unlike the Xilokastro fault farther east, no re-

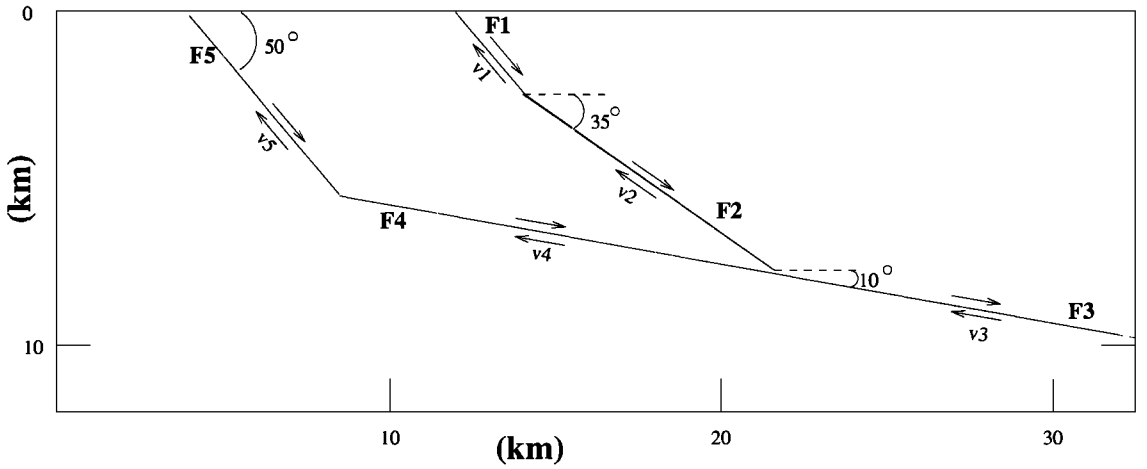

Figure 12. Five-fault model used in the modeling. Location of the five fault segments is discussed in the text and is based on the observed active structures along the A-G profile. Each fault F_i has a slip rate v_i.

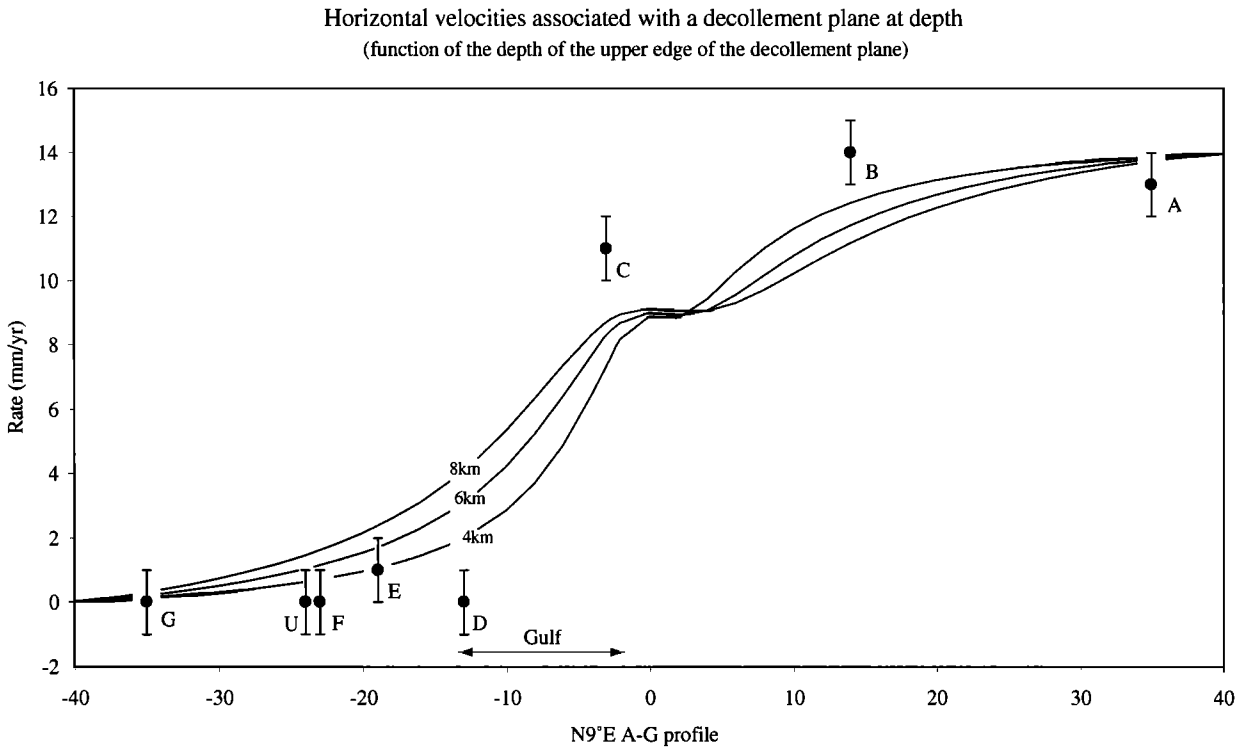

Figure 13. Horizontal velocities predicted by a 10° north dipping decollement located at three different depths (4, 6, and 8 km, with the upper edge of the plane located at x=0 km). For each depth, the slip velocity is adjusted in order to obtain 14 mm/yr between G and A. Note that even a very shallow decollement is unable to explain the observations.

liable estimate of the long-term slip rate exists for the Helike fault. However, on the basis of terrace uplift analysis, *Rigo* [1994] estimated that the slip on the Helike fault could be at least half that on the Xilokastro fault, that is 3-4 mm/yr. We thus present two different models corresponding to two different hypothesis for partitioning (Figure 14): model 1a (Table 5) has 10 and 4 mm/yr of opening on the inner and southern faults, respectively, and model 1b (Table 6) has equal opening rates on the inner and southern faults. A good

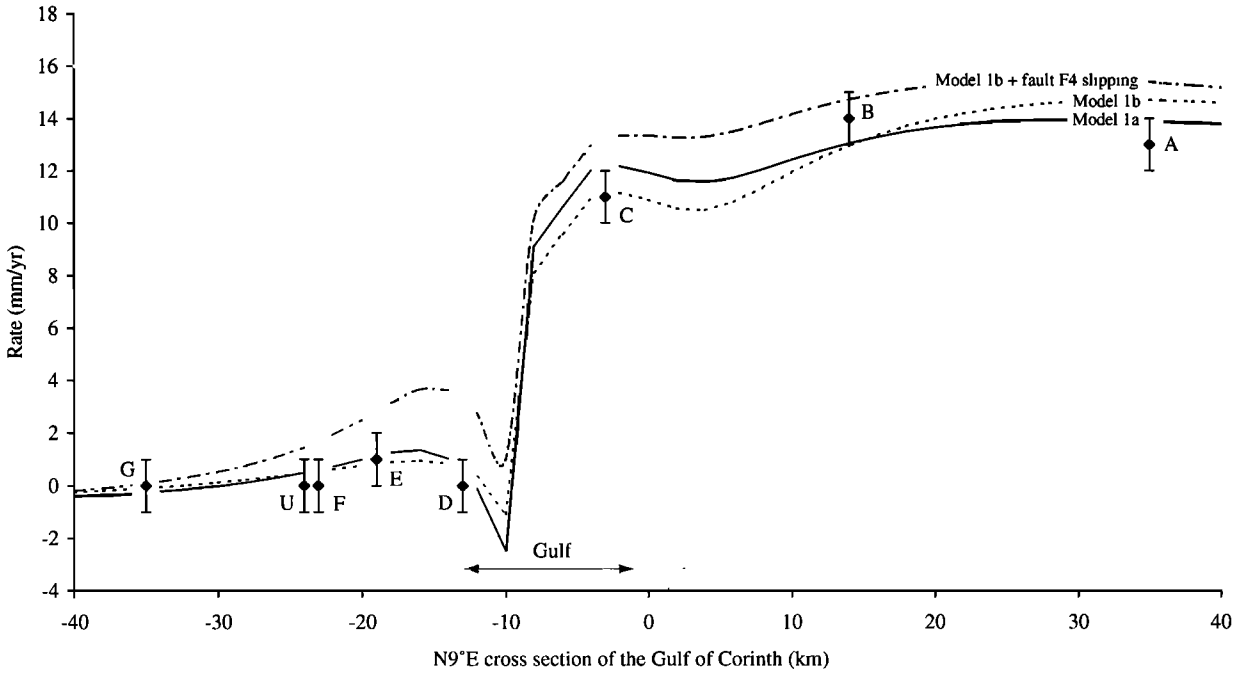

Figure 14. Comparison of observed and modeled interseismic extension rates along line A-G for the two models discussed in the text. Model 1a (Table 5) corresponds to an average 4 mm/yr of slip on the Helike fault and model 1b (Table 6) corresponds to 7 mm/yr.

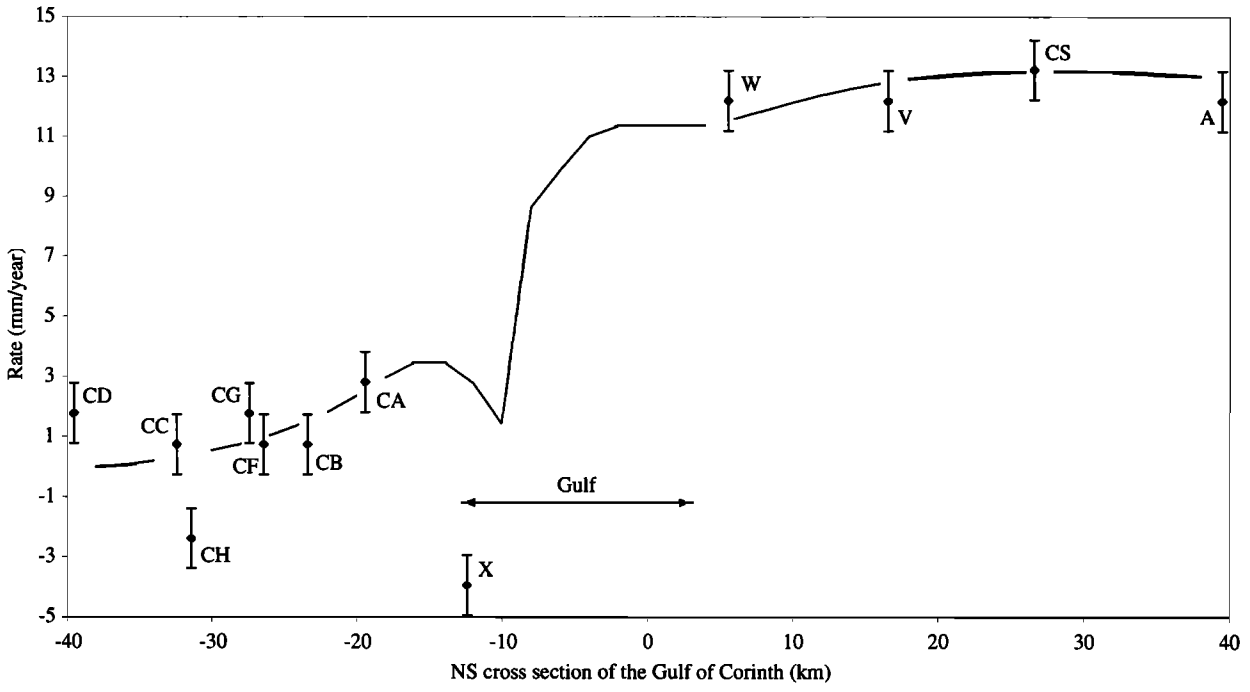

Figure 15. Comparison of observed and modeled extension rates along line CS-CD. The model assumes an average 7 mm/yr of slip on the Xilokastro fault (Table 7, model 2).

fit of the GPS observations and, in particular, the narrow deforming zone is obtained with model 1a if F4 is assumed to slip in a continuous mode. We checked that the solution does not change significantly when the angle of faults F3-F4 varies between 0° and 20°. This model predicts recurrence times of 242±60 years for the Helike fault and of 71±7 years for the offshore faults.

Model 1b assumes opening rates of 7 mm/yr on both fault segments. Figure 14 shows that the fit to the data is poor when continuous slip is assumed on the upper decollement (fault F4). To fit the data, this fault needs to behave in a brittle-elastic manner instead of in a creeping mode. This solution, however, implies a rate of seismic moment about twice that required for partitioning at 10 and 4 mm/yr. This is thus in poor agreement with the seismic rates deduced from the seismicity as discussed in section 5.

4.2. Xilokastro Profile (Line CS-CD)

Existing constraints for this profile are the opening rate deduced from the GPS data (13 mm/yr) and the horizontal opening rate across the Xilokastro fault (7±2 mm/yr) measured over geological timescale [*Armijo et al.*, 1996]. Assuming the same geometry for the faults as that used for the A-G line and the same characteristic earthquakes, the predicted opening rates across the rift are plotted in Figure 15. The parameters of the model are detailed in Table 7. The fit with the extrapolated

Table 5. Model 1a (Aigion Area) With 4 mm/yr Extension Rate on Southern Faults and 10 mm/yr on Inner-Rift Faults

Fault	Rate, mm/yr	Slip per earthquake, mm	Fault lenght, km	Recurrence time, years	M_s geodetic,	M_o, 10^{18} N m	M_o/100 years/15 km, 10^{18} N m
F1	15.6						
F2	12.2	870	15	71	6.35	3.9	5.5
F3	14.2						
F4	4.1						
F5	6.2	1500	25	242	6.7	8.7	2.2

The slip rates are deduced from the assumed geometry and the adopted slip balance of 10 and 4 mm/yr for inner gulf faults and southern gulf faults. The Aigion earthquake is assumed to be characteristic for F2. The recurrence time on the inner rift fault plane is deduced from the comparison of the model and the 1990-1994 data. We use the relation $\log(M_o)=12.24 + M_s$. The typical M_s on the southern fault F5 is assumed to be 6.7. This corresponds to a seismic slip of 1.5 m on a 25-km-long segment, which roughly corresponds to the observed offsets and fault length of the 1861 Helike earthquake. The recurrence times on the faults are deduced from the slip rate and the assumed coseismic offsets (870 mm and 1500 mm, respectively).

Table 6. Model 1b (Aigion Area) With 7 mm/yr Extension Rate on Southern Faults and 7 mm/yr on Inner-Rift Faults

Fault	Rate, mm/yr	Slip per earthquake, mm	Fault lenght, km	Recurrence time, years	M_s geodetic,	M_o, 10^{18} N m	M_o/100 years/15 km, 10^{18} N m
F1	10.9						
F2	8.5	870	15	102	6.35	3.9	3.9
F3	14.2						
F4	7.1	975	25	138			
F5	10.9	1500	25	138	7.05	19.3	13.6

It is not possible to fit the data when continuous slip is assumed on the upper decollement F4. The total seismic moment related to this model is 2 times larger than that corresponding to model 1a. The recurrence time on the southern faults is not compatible with the record of large earthquakes in the gulf, and the predicted magnitude is too large with respect to the typical magnitude of earthquakes in the gulf.

1993-1995 rate is good. The typical recurrence time for the earthquakes in this area is longer for the offshore faults (119±20 years) and shorter for the southern faults (138±20 years) than that estimated for the Aigion area.

5. Discussion and Implications for the Deformation of the Corinth Rift

5.1. Energy Release in the Corinth Rift

A direct output of the models presented is the estimate of rates of seismic moment release along the profiles A-G and CS-CD. In order to calculate the predicted seismic moment release rate for the entire length of the rift we first calculated the predicted seismic moment release rate for 15-km-long segments for both the Aigion and Xilokastro profiles (Table 8). Assuming a mean rate of 12±2 mm/yr of extension for the entire rift and taking into account the fact that eight 15-km-long segments are needed for the entire rift, the total seismic moment rate estimate is 53±9 x 10^{16} N m/yr. This is to be compared to the 42 x 10^{16} N m/yr obtained by *Ambraseys and Jackson* [1990] from seismic moment tensor summation of the last century. Assuming a seismogenic layer thickness between 10 and 15 km, *Clarke et al.* [1997] found values of 85±15 x 10^{16} N m/yr. In our modeling, the effective seismogenic layer is 10-12 km outside the gulf and only about 7-8 km beneath the gulf. It is thus logical that our seismic moment rate be somewhat smaller than the value estimated by *Clarke et al.* [1997]. Two sets of observations argue in favor of a thin seismogenic layer beneath the gulf. A detailed microearthquake study carried out in the western part of the Corinth rift [*Rigo et al.*, 1996] located no earthquake deeper than 12 km in the area and no earthquake deeper than 10 km beneath the gulf itself. On the other hand, the lack of seismicity in the upper 3-4 km of the crust is also evident in Rigo et al.'s study. Although it is difficult to reject the fact that this may be an artifact due to the hypocenter selection criteria, *Bernard et al.* [1997a] came up with the same conclusion for the Aigion earthquake that on the basis of deformation and aftershock data, this event did not rupture the upper 4 km beneath the gulf. *Cattin et al.* [1999] have shown that for a Young's modulus contrast of 10 between superficial layers and crustal material below, the superficial layers simply follow the elastic deformation of the crust below, meaning that the superficial layers do not contribute to the effective elastic thickness in this case [see also *Savage*, 1998]. We think that the thin seismogenic

Table 7. Model 2 (Xilokastro Area) With 6 mm/yr Extension Rate on Southern Faults and 7 mm/yr on Inner-Rift Faults

Fault	Rate, mm/yr	Slip per earthquake, mm	Fault lenght, km	Recurrence time, years	M_s geodetic,	M_o, 10^{18} N m	M_o/100 years/15 km, 10^{18} N m
F1	9.3						
F2	7.3	870	15	119	6.35	3.9	3.3
F3	13.2						
F4	7.1						
F5	10.9	1500	25	138	6.7	8.7	3.8

We assume that typical inner rift earthquakes are similar to the June 15, 1995, Aigion earthquake, with average slip on fault 870 mm. The recurrence time is longer than in the Aigion area due to the lower opening rate across the gulf here.

Table 8. Estimated Values of Seismic Moment Release in the Corinth Rift

Segment	Rate, mm/yr	Inner Gulf	Southern Faults	Total	Clarke et al.	Seismic
Aigion	14	5.5 ± 0.5	2.2 ± 0.5	7.7 ± 1		
Recurrence time, years		71 ± 7	242 ± 60			
Xilokastro	13	3.3 ± 0.5	3.8 ± 0.5	7.1 ± 1		
Recurrence time, years		119 ± 20	138 ± 20			
All (eight)	12 ± 2[a]			52 ± 10	85 ± 15	42 ± 18[b]

Value of μ used is 3.3 x 10^{10} N m^{-2}. The seismic moments in Aigion and Xilokastro areas are computed for a 15-km length zone. Our estimate is 1.5 to 2 times lower than that of *Clarke et al.* [1997] and close to the value found by *Ambraseys and Jackson* [1990]. Error estimates on the recurrence times are internal errors of the modeling itself, assuming no errors on the extension rate. All moments are in units of 10^{18} N m/100 years.

[a]Average value for the whole Corinth rift.

[b]Seismic moment release estimated by *Ambraseys and Jackson* [1990].

layer in the Corinth rift is due both to the fairly shallow depth of the brittle-ductile transition (10-12 km) and to the presence of relatively thick (2-4 km) unconsolidated sediments within the gulf below 0.5 to 0.8 km of water. The other factor that contributes to the reduction of our estimate of seismic moment rate is the fact that we introduced seismic faults with low dips in our modeling. For a given seismic moment, the amount of extension will be ~25% larger if slip occurs on a 30° dipping fault rather than on a 50° dipping fault. *Ambraseys and Jackson* [1997] evaluated the opening velocity deduced from earthquakes of magnitudes larger than 6 over the last 300 years and concluded that it may be 5-10% larger than the velocity estimates based on only 100 years of seismicity [*Ambraseys and Jackson*, 1990]. This indicates that the seismic moment rate release calculated over 300 years is not significantly different from that calculated over 100 years. Our estimate based on deformation modeling is quite close to *Ambraseys and Jackson*'s [1990] determination. This indicates that if our assumption of creep at shallow depth is valid, there is no need to invoke aseismic strain at midcrustal depths.

5.2. Partitioning of the Deformation and Recurrence Time of Earthquakes

Our modeling predicts that 71% of the energy release across the Corinth rift at the longitude of Aigion is associated with earthquakes in the inner part of the Corinth rift. On average, for the entire rift we find that $\geq$ 50% of the energy is released in the inner Gulf of Corinth. In terms of contribution to the long-term extension of the Corinth rift, the contribution of the extension located off shore to the total extension is also $\geq$ 50%. As we discussed above, we suggest that the contribution of the earthquakes located in the inner Corinth rift to its extension is increased by two factors: first, the fact that the seismogenic thickness is reduced there (presence of water and unconsolidated sediments at the top of the upper crust there); and second, the fact that faults have lower dip angle there and thus accommodate more extension for a given energy release. In our model the predicted recurrence times for magnitude 6.7 earthquakes on the main faults bordering the southern Gulf of Corinth are typically 138-242 years. For the entire Gulf of Corinth, *Ambraseys and Jackson* [1997] listed eight events of magnitude $\geq$ 6.5 in the last 300 years that could correspond to this type of event. This suggests that the modeled recurrence time of 242±60 years (Aigion) is possible but that 138±20 years (Xilokastro) is probably too small. Alternatively, the energy may be partly released there by smaller-magnitude earthquakes or the assumed slip rate on the Xilokastro fault is too large.

6. Conclusion

The GPS data analyzed in this study show that the Corinth rift is extending at rates ranging between 14 mm/yr in the west and 10 mm/yr in the east. The density of our observations allows us to show that the deformation is localized in a very narrow deforming zone, in particular, in the western part of the rift where strain rates reach values of 4.5 x 10^{-14} s^{-1}. Assuming that this high rate over 5 years represents the steady state deformation across the rift, we propose a simple model of fault partitioning that explains the GPS observations and is consistent with available seismological and tectonic observations. In our model a large part of the seismic deformation is localized on relatively low-angle faults located off shore at depth ranging between 4 and 10 km, and the upper crust located above this depth deforms mostly in a creeping mode. This thickness of 4 km could represent the total thickness of the layer constituted by the water (0.5-0.8 km), the young sediments of the gulf (2-4 km depending on areas), and the uppermost fractured rocks located below the young sediments (1 km). Below 10 km, the deformation is modeled as creep along a decollement suggested by seismological studies [*Rigo et al.*, 1996; *Rietbrock et al.*, 1996]. The important implication is that only about one half of the observed deformation, and even less in the western

part of the gulf, is stored as elastic energy in the seismogenic layer. If this is true, the particularly high observed strain rate in the central and western part of the gulf does not imply a large deficit of seismic energy release as proposed by *Clarke et al.* [1997]. In the easternmost part of the gulf, where the strain rate is smaller, no low dip normal faults are known. The percentage of the deformation stored as elastic energy could be larger than in the central and western part of the gulf and close to 100%, as proposed by *Clarke et al.* [1997]. This is confirmed by the coseismic calculations shown on Figure 10. One difficulty with the model proposed here, where a large part of the deformation occurs within the gulf on low-dipping faults, concerns the prediction of vertical movements. A detailed investigation of this problem is beyond the scope of this paper, but it is unlikely that the model we propose can explain the topography of the rift flanks in the Aigion area. One possibility is that the faulting conditions changed fairly recently related in particular to an increase in strain rate. Faulting may have started and may have continued for some time at high angle. As proposed by *Melosh* [1990], low-angle faulting may evolve from high-angle faults due to stress rotation associated with a low-viscosity lower crust. Evidence for such a low-viscosity lower crust at 10 km below the Gulf of Corinth comes from magnetotelluric observations indicating an extremely conductive layer below 10 km suggesting a ductile rheology with possibly fluid-enriched rocks [*Pham et al.*, 1996]. Further investigation of this problem should involve numerical modeling with a realistic depth dependent rheology as proposed by *Hassani and Chéry* [1996]. Recently, *Hager et al.* [1999] have shown that steep gradients of deformation (somewhat smaller than those observed here) could be explained in part by a viscoelastic model with lateral variations of elastic modulus, which favors the localization of elastic strain in the more compliant region. It would be interesting to discuss such a possible mechanism for the Corinth rift to estimate how it could localize the deformation and in which conditions this could be an alternative model to creeping at shallow depth as proposed here.

Acknowledgments. More than 60 people participated in one or more GPS campaigns. We thank all of them. R. Armijo participated in the initiation of the project and the network design. This work benefited from several discussions with P. Bernard and J. Chéry. We thank Barry Parsons, John Beavan, and an anonymous reviewer for their comments and suggestions. This work was supported by CE EPOC CT 91-0043 program, CNRS/INSU DBT, IDYL, PNRN programs, and Greek-French PLATON program. IPGP contribution 1697.

References

Ambraseys, N.N., and J.A. Jackson, Seismicity and associated strain of central Greece between 1890 and 1988, *Geophys. J. Int., 101,* 663-708, 1990.

Ambraseys, N.N., and J.A. Jackson, Seismicity and strain in the Gulf of Corinth (Greece), *J. Earthquake Eng., 1(3),* 433-474, 1997.

Anzidei, M., P. Baldi, G. Casula, M. Crespi, and F. Riguzzi, Repeated GPS surveys across the Ionian Sea: evidence of crustal deformations, *Geophys. J. Int., 127,* 257-267, 1996.

Armijo, R., B. Meyer, G. King, A. Rigo, and D. Papanastassiou, Quaternary evolution of the Corinth rift and its implications for the late Cenozoic evolution of the Aegean, *Geophys. J. Int., 126,* 11-53, 1996.

Baker, C., D. Hatzfeld, H. Lyon-Caen, E. Papadimitriou, and A. Rigo, Earthquake mechanisms of the Adriatic sea and western Greece: Implications for the oceanic subduction-continental collision transition, *Geophys. J. Int., 131,* 559-594, 1997.

Bernard, P., et al., The M_s=6.2, June 15, 1995 Aigion earthquake (Greece): Evidence for low angle normal faulting in the Corinth rift, *J. Seismol., 1,* 131-150, 1997a.

Bernard, P., M. Chouliaras, A. Tzanis, P. Briole, M.P. Bouin, J. Tellez, G. Stavrakakis, and K. Makropoulos, Seismic and electrical anisotropy in the Mornos delta, Gulf of Corinth, Greece, and its relationship with GPS strain measurements, *Geophys. Res. Lett., 24,* 2227-2230, 1997b.

Billiris, H., et al., Geodetic determination of tectonic deformations in Greece from 1900 to 1988, *Nature, 350,* 124-129, 1991.

Boucher, C., and Z. Altamimi, ITRF89 and other realizations of the IERS Terrestrial Reference System for 1989, *IERS Tech. Rep., 6,* 1989.

Boucher, C., Z. Altamimi, and L. Duhem, ITRF92 and its associated velocity field, edited by S.O. Dickey and M. Feissel, *IERS Tech. Note, 15,* Obs. de Paris, 1993.

Briole, P., A. Deschamps, H. Lyon-Caen, K. Papazissi, and J. Martinod, The Itea (M_s=5.9) earthquake of November 18, 1992: Characteristics of the main shock inferred from body wave and ground displacement analysis, paper presented at 2nd Hellenic Geophysical Union, Florina, Greece, May 1993.

Cattin, R., P. Briole, H. Lyon-Caen, P. Bernard, and P. Pinettes, Effects of superficial layers on coseismic displacements for a dip-slip fault and geophysical implications, *Geophys. J. Int., 137,* 149-158, 1999.

Clarke, P.J., et al., Geodetic estimation of seismic hazard in the Gulf of Corinth, *Geophys. Res. Lett., 24,* 1303-1306, 1997.

Clarke, P.J., et al., Crustal strain in central Greece from repeated GPS measurements in the interval 1989-1997, *Geophys. J. Int., 135,* 195-214, 1998.

Davies, R.R., P.C. England, B. Parsons, H. Billiris, D. Paradissis, and G. Veis, Geodetic strain of Greece in the interval 1892-1992, *J. Geophys. Res., 102,* 24,571-24,588, 1997.

Denys, P., et al., GPS networks for determining the accumulation of current crustal strain in central Greece, paper presented at 1st International Symposium on Deformation in Turkey, Istambul Technical University, Istambul, Turkey, 1994.

Gilbert, L.E., C.H. Scholz, and J. Beavan, Strain localization along the San Andreas fault: Consequences for loading mechanisms, *J. Geophys. Res., 99,* 23,975-23,984, 1994.

Hager, B., G. Lyzenga, A. Donnellan, and D. Dory, Reconciling rapid strain accumulation with deep seismogenic fault planes in the Ventura Basin, California, *J. Geophys. Res., 104,* 25,207-25,219, 1999.

Hassani, R., and J. Chéry, Anelasticity explains topography associated with Basin and Range normal faulting, *Geology, 24,* 1095-1098, 1996.

Hatzfeld, D., et al., The Galaxidi earthquake of November 18, 1992: A possible asperity within the normal fault system of the Gulf of Corinth (Greece), *Bull. Seismol. Soc. Am., 86,* 1987-1991, 1996.

Hubert, A., G.C.P. King, R. Armijo, and B. Meyer, Fault reactivation, stress interaction and rupture propagation in the 1981 Corinth earthquake sequence, *Earth Planet. Sci. Lett., 142,* 573-586, 1996.

Jackson, J.J., and D. McKenzie, The relationship between plate motions and seismic moment tensors and the rate of active deformation in the Mediterranean and the Middle East, *Geophys. J., 93,* 45-73, 1988.

Jackson, J.J., J. Gagnepain, G. Houseman, G. King, P. Papadimitriou, P. Soufleris, and J. Virieux, Seismicity, normal faulting and the geomorphological development of the Gulf of Corinth (Greece): The Corinth earthquakes of February and March 1981, *Earth Planet. Sci. Lett., 57,* 377-397, 1982.

Kahle, H.G., M.V. Muller, A. Geiger, G. Danuser, S. Mueller, G. Veis, H. Billiris, and D. Paradissis, The strain field in NW Greece and the Ionian Islands: Results inferred from GPS measurements, *Tectonophysics, 23,* 677-680, 1995.

King, G.C.P., D. Oppenheimer, and F. Amelung, Block versus continuum deformation in the western United States, *Earth Planet. Sci. Lett., 128,* 55-64, 1994.

Le Pichon, X., and J. Angelier, The Aegean sea, *Philos. Trans. R. Soc. London, Ser. A, 300,* 357-372, 1981.

Le Pichon, X., N. Chamot-Rooke, S. Lallemant, R. Noomen, and G. Veis, Geodetic determination of the kinematics of central Greece with respect to Europe: Implications for eastern Mediterranean tectonics, *J. Geophys. Res., 100,* 12,675-12,690, 1995.

McKenzie, D.P., Active tectonics of the Alpine-Himalayan belt: The Aegean Sea and surrounding regions, *Geophys. J. R. Astron. Soc., 55,* 217-254, 1978.

Melosh, H.J., Mechanical basis for low-angle normal faulting in the Basin and Range province, *Nature, 343,* 331-335, 1990.

Mercier, J.L., E. Carey, H. Philip, and D. Sorel, La néotectonique plio-quaternaire de l'arc Egéen externe et de la mer Egée et ses relations avec la sismicité, *Bull. Soc. Geol. Fr., 18,* 159-176, 1977.

Papazachos, B.C., and C.B. Papazachos, *The Earthquakes of Greece* (in Greek), 356 pp., Ziti Thessaloniki, Greece, 1989.

Pham, V.N., D. Boyer, G. Chouliaras, and P. Bernard, Conductivité électrique et structure de la croûte dans la région du Golfe de Corinthe (Grèce) d'après les résultats de sondage magnétotellurique (SMT), *C. R. Acad. Sci., Ser. II, 323,* 651-656, 1996.

Rietbrock, A., C. Tiberi, F. Scherbaum, and H. Lyon-Caen, Seismic slip on a low angle normal fault in the Gulf of Corinth: Evidence from high-resolution cluster analysis of microearthquakes, *Geophys. Res. Lett., 23,* 1817-1820, 1996.

Rigo, A., Etude sismotectonique et geodesique du Golfe de Corinthe (Grece), Ph.D. thesis, Univ. Paris VII, 1994.

Rigo, A., H. Lyon-Caen, R. Armijo, A. Deschamps, D. Hatzfeld, K. Makropoulos, P. Papadimitriou, and I. Kassaras, A microseismic study in the western part of the Gulf of Corinth (Greece): Implications for large-scale normal faulting mechanisms, *Geophys. J. Int., 126,* 663-688, 1996.

Ruegg, J.C., and C. Bougault, AG3D, Notice d'utilisation, *IPGP report,* 32 pp., Inst. de Phys. du Globe de Paris, 1992.

Savage, J.C., Displacement field for an edge dislocation in a layered half-space, *J. Geophys. Res., 103,* 2439-2446, 1998.

Sébrier, M., Tectonique récente d'une transversale à l'Arc Egéen: Le golfe de Corinthe et ses régions périphériques, thèse de 3e cycle, Univ. Paris-Sud, Orsay, France, 1977.

Tarantola, A., and B. Valette, Generalized nonlinear inverse problem solved using the least squares criterion, *Rev. Geophys., 20,* 219-232, 1982.

Taymaz, T., J.A. Jackson, and D. McKenzie, Active tectonics of the north and central Aegean Sea, *Geophys. J. Int., 106,* 433-490, 1991.

Veis, G., H. Billiris, B. Nakos, and D. Paradissis, Tectonic strain in Greece from geodetic measurements, *Proc. Athens Acad., 67,* 129-166, 1992.

A. Balodimou, C. Mitsakaki, K. Papazissi, and G. Veis, Higher Geodesy Laboratory, National Technical University, Athens, 9 Heroon Polytechniou str., GR-15780 Zographos, Greece. (ambal@central.ntua.gr; topocris@central.ntua.gr; topoepy@central.ntua.gr; veis@softlab.ece.ntua.gr)

P. Briole, and J.C. Ruegg, Département de Sismologie, UMR-CNRS 7580, Institut de Physique du Globe de Paris, 4 place Jussieu, F-75252 Paris Cedex 05, France. (briole@ipgp.jussieu.fr; ruegg@ipgp.jussieu.fr)

A. Deschamps, Laboratoire de Géodynamique, UMR Geosciences Azur, CNRS Sophia-Antipolis 1, 250 avenue Albert Einstein, F-06560 Valbonne, France. (deschamp@faille.unice.fr)

D. Hatzfeld, Laboratoire de Géophysique Interne et Tectonophysique (LGIT), UMR-CNRS 5559, Observatoire de Grenoble, BP 53, F-38041 Grenoble Cedex 09, France. (hatzfeld@obs.ujf-grenoble.fr)

H. Lyon-Caen, Laboratoire de Géologie, UMR-CNRS 8535, Ecole Normale Supérieure, 24 rue Lhomond, F-75231 Paris Cedex 05, France. (helene.lyon-caen@ens.fr)

A. Rigo, Observatoire Midi-Pyrénées, Groupe de Recherche en Géodesie Spatiale (GRGS), UMR-CNRS 5562, 14 avenue Edouard Belin, F-31400 Toulouse, France. (alexis.rigo@cnes.fr)

(Received August 5, 1999; revised April 7, 2000;
accepted April 18, 2000.)